DEVELOPMENT OF A FAST ANALYTICAL METHOD FOR PREDICTION OF PART DYNAMICS IN MACHINING STABILITY ANALYSIS

A THESIS SUBMITTED TO
THE GRADUATE SCHOOL OF NATURAL AND APPLIED SCIENCES
OF
MIDDLE EAST TECHNICAL UNIVERSITY

BY

SALİH ALAN

IN PARTIAL FULFILLMENT OF THE REQUIREMENTS
FOR
THE DEGREE OF MASTER OF SCIENCE
IN
MECHANICAL ENGINEERING

SEPTEMBER 2009

Approval of the thesis:

DEVELOPMENT OF A FAST ANALYTICAL METHOD FOR PREDICTION OF PART DYNAMICS IN MACHINING STABILITY ANALYSIS

submitted by **SALİH ALAN** in partial fulfillment of the requirements for the degree of **Master of Science in Mechanical Engineering Department, Middle East Technical University** by,

Prof. Dr. Canan Özgen _____
Dean, Graduate School of **Natural and Applied Sciences**

Prof. Dr. Suha Oral _____
Head of Department, **Mechanical Engineering**

Prof. Dr. H. Nevzat Özgüven _____
Supervisor, **Mechanical Engineering Dept., METU**

Assoc. Prof. Dr. Erhan Budak _____
Co-Supervisor,
Faculty of Engineering and Natural Sciences,
Sabancı University

Examining Committee Members:

Prof. Dr. Mehmet Çalışkan _____
Mechanical Engineering Dept., METU

Prof. Dr. H. Nevzat Özgüven _____
Mechanical Engineering Dept., METU

Assoc. Prof. Dr. Erhan Budak _____
Faculty of Engineering and Natural Sciences,
Sabancı University

Prof. Dr. S. Engin Kılıç _____
Mechanical Engineering Dept., METU

Asst. Prof. Dr. Ender Ciğeroğlu _____
Mechanical Engineering Dept., METU

Date: 09.09.2009

I hereby declare that all information in this document has been obtained and presented in accordance with academic rules and ethical conduct. I also declare that, as required by these rules and conduct, I have fully cited and referenced all material and results that are not original to this work.

Name, Last name : Salih ALAN

Signature :

ABSTRACT

DEVELOPMENT OF A FAST ANALYTICAL METHOD FOR PREDICTION OF PART DYNAMICS IN MACHINING STABILITY ANALYSIS

Alan, Salih
M.S., Department of Mechanical Engineering
Supervisor: Prof. Dr. H. Nevzat Özgüven
Co-Supervisor: Assoc. Prof. Dr. Erhan Budak

September 2009, 87 pages

The objective of this study is to develop and implement practical and accurate methods for prediction of the workpiece dynamics during a complete machining cycle of the workpiece, so that FRFs of the workpiece can be used in chatter stability analysis. For this purpose, a structural modification method is used since it is an efficient tool for updating FRFs due to structural modifications. The removed mass is considered as a structural modification to the finished workpiece in order to determine the FRFs at different stages of the process. The method is implemented in a computer code and demonstrated on representative parts such as turbine blades. The predictions are compared and verified with the data obtained using FEA. The FRFs are used in chatter stability analyses, and the effect of part dynamics on stability is studied.

Keywords: Chatter Vibrations, Chatter Stability, Structural Dynamics, Structural Modification, Finite Element Formulation.

ÖZ

METAL İŞLEMENİN KARARLILIK ANALİZİNDE PARÇA DİNAMİĞİNİN TAHMİNİ İÇİN HIZLI ANALİTİK BİR YÖNTEMİN GELİŞTİRİLMESİ

Alan, Salih
Yüksek Lisans, Makine Mühendisliği Bölümü
Tez yöneticisi: Prof. Dr. H. Nevzat Özgüven
Yardımcı tez yöneticisi: Doç. Dr. Erhan Budak

Eylül 2009, 87 sayfa

Bu çalışmadaki amaç, metal işlemede, bir parçanın bütün işleme çevrimindeki dinamiğinin tahmin edilmesi için pratik ve doğru yöntemlerin geliştirilmesi ve uygulanmasıdır. Bu amaçla, yapısal değişimden etkilenen FTF'lerin yeni değerlerinin bulunmasında verimli bir araç olan bir yapısal değişim yöntemi kullanılmıştır. İşleme esnasındaki kütle kaldırılmasını işlenen parçadaki yapısal değişim olarak değerlendirerek, farklı işleme aşamalardaki FTF'ler hesaplanabilir. Yöntem, bir bilgisayar yazılımıyla gerçekleştirilmiştir ve türbin kanatçıkları gibi tipik parçalarda uygulanmıştır. Teorik sonuçlar, sonlu elemanlar analizinden elde edilen sonuçlarla karşılaştırılmış ve doğrulanmıştır. Bu FTF'ler kararlılık analizlerinde kullanılmış ve parça dinamiğinin kararlılık üzerindeki etkisi incelenmiştir.

Anahtar kelimeler: Tırlama Titreşimleri, Tırlama Kararlılığı, Yapı Dinamiği, Yapısal Değişiklik, Sonlu Elemanlar.

To my family

ACKNOWLEDGEMENTS

I would like to express my sincere gratitude to my supervisors, Prof. Dr. H. Nevzat Özgüven and Assoc. Prof. Erhan Budak, for their invaluable supervision, advice, criticism and support that made the study possible.

The discussions with Asst. Prof. Dr. Ender Ciğeroğlu are gratefully acknowledged. I would like to thank research assistant L. Taner Tunç of Sabancı University for the discussions with him.

The first editing of the whole text by my friend Bekir Bediz is appreciated. I would also like to thank my friends and colleagues, mostly to Özlem Demirkan, Tuğçe Yüksel, Ali Murat Kayıran, Hakan Çalışkan, M. Ural Uluer and Z. Murat Kılıç, for their help and support.

I would like to thank my family for their support and patience.

The study is supported by TÜBİTAK under the project number 108M340.

TABLE OF CONTENTS

LIST OF FIGURES

FIGURES

LIST OF TABLES

TABLES

LIST OF SYMBOLS

a_i	: Nodeless degrees of freedom
$a_{\text{lim},i}$	: Limiting axial depth of cut at i^{th} step
$[B]$	: Strain-displacement relation matrix
b_{lim}	: Limiting depth of cut
$\det[\ ]$	: Determinant of a matrix
$[D]$	: Dynamic structural modification matrix
$[E]$	: Elasticity matrix
E	: Modulus of elasticity
f	: Feed rate per flute
$\{F\}$	: Forcing vector
FEA	: Finite element analysis
FRF	: Frequency response function
FRF_{xx}	: FRF for displacement and loading in x direction
$G(\omega)$	: FRF of the system
$[H]$	: Structural damping matrix
H_i	: Weighting factor for i^{th} sampling point
i	: Unit imaginary number
$[I]$	: Identity (unit) matrix
$[J]$	: Jacobian matrix
$[K]$	: Stiffness matrix
K_s	: Cutting force coefficient

$[K_{ij}]$: Elements of the stiffness matrix

$[L]$: Inverse of Jacobian matrix

$L_{ax,i}$: Length of i^{th} step of the blade in axial direction

$L_{f,i}$: Length of i^{th} step of the blade in feed direction

m : Number of sampling points

$[M]$: Mass matrix

n : Spindle speed

nop_i : Number of passes required at i^{th} step

$[N]$: Shape function matrix

N : Number of flutes on the cutter

N_i : i^{th} shape function

P_i : i^{th} integration point

$\{Q\}$: Forcing vector

t : Machining time

u, v, w : Displacements in x, y, z directions

u_i, v_i, w_i : Displacements in x, y, z directions at i^{th} node

V_f : Feed rate

w : Width of the workpiece

x_i, y_i, z_i : Nodal coordinates in the global coordinate system

$\{x\}$: Displacement vector

$\{\dot{x}\}$: Velocity vector

$\{\ddot{x}\}$: Acceleration vector

$[\alpha]$: Receptance matrix of the original system

α_{ij} : Submatrix of the receptance matrix for the original system

$[\gamma]$: Receptance matrix for the modified system

γ_{ij} : Submatrix of the receptance matrix for the modified system

γ_{ij} : Normal strain

γ_r : Damping coefficient of r^{th} mode

$\{\delta\}$: Nodal displacement vector

$\frac{\partial}{\partial x}$: Partial differentiation with respect to x

$\{\Delta\}$: Displacement vector

$[\Delta M]$: Modification mass matrix

$[\Delta H]$: Modification structural damping matrix

$[\Delta K]$: Modification stiffness matrix

$\{\varepsilon\}$: Strain vector

ε_i : Longitudinal strain

$\{\phi_i^r\}$: Elements of r^{th} mode shape vector

ξ, η, ζ : Natural coordinates

ρ : Density

ν : Poisson's ratio

ω : Excitation frequency

ω_r : r^{th} natural frequency

CHAPTER 1

INTRODUCTION

1.1 Objective

Machining vibrations develop due to the relative motion between the tool and the workpiece. Even though both tool and workpiece may contribute to the relative displacement, in general, only the dynamics of the tool is considered in the stability analysis, and the dynamics of the workpiece is neglected. Although this can be considered as a valid approach for cases where the workpiece is much stiffer than the tool, for cases where the workpiece is relatively flexible, part dynamics should also be taken into account in the calculation of the frequency response functions (FRF). For those cases neglecting the effect of part dynamics may result in significant errors in stability predictions.

For a flexible workpiece, FRFs of the part are required to be known for all stages of the machining cycle. Part dynamics prior to and after machining can be determined by experimental techniques or finite element analysis. However, it would not be practical to use these methods for each stage of manufacturing as the part geometry, and thus the dynamics, vary continuously. In this study, a structural modification technique is employed to predict the part dynamics during a complete machining cycle. In the method applied, the effect of removed material on the workpiece dynamics

is considered. Based on the practical methodology presented, chatter stability analysis and predictions can be performed more accurately by considering the complete structural dynamics in a machining system.

1.2 Literature Review

Chatter is undesired self-excited vibrations between the machine tool and the workpiece. It may yield important problems like poor surface finish, tool wear and fracture, damage to the machine and lower productivity. Previous research revealed that there are two basic reasons for chatter: regenerative effect and mode coupling effect. The regenerative chatter can be explained as the vibration induced by the phase shift between the surfaces generated in successive passes on the same surface [1]. Mode coupling effect is present for the cases in which there are relative motions between the tool and the part in two directions [2]. Since the stability limit for regenerative chatter is lower than the one for the mode coupling, regenerative chatter is considered in machining stability analyses.

The theory of prediction of chatter vibration was established by Tobias and Fishwick [3, 4]. For the turning chatter problem, they built a mathematical theory and proposed the stability chart approach which gives the stability conditions for a given cutting system. Later, the regenerative effect was modeled using the feedback control theory by Merritt [5] and stability boundaries of the cutting process were calculated. Application of the receptance function to chatter prediction was offered by Tlusty [6]. He used the receptance of the motion between the tool and the workpiece, and

developed a stability law for orthogonal cutting, which gives the limit of axial depth of cut without chatter for different cutting speeds.

The mechanics for milling is much complicated than other processes, since as the cutting tool rotates, the directions of the loadings and the vibrations change. Minis and Yanushevski [7, 8] formulated the chatter in milling using the Floquet's theorem and Fourier series and determined the stability limits numerically using Nyquist stability criterion. Altıntaş and Budak [9-11] presented an analytical frequency based method for the stability prediction of milling and applied this method to predict the stability of different milling systems.

Stability lobe theory is developed as a remedy for the chatter problem. In this theory, the chatter stability is predicted by analytical methods. The stable depths of cut are calculated for different spindle speeds and stability lobe diagram is plotted. The equation for the limiting depth of cut, i.e. the maximum chatter-free depth of cut, is given in by Tlusty [2] as:

$$b_{\lim} = \frac{-1}{2 \cdot K_s \cdot \mathrm{Re}\left(G(\omega)\right)} \tag{1.1}$$

where K_s is the cutting force coefficient in the chip direction, relating the cutting force and the cutting area, and $G(\omega)$ is the FRF of the system. If the part dynamics is neglected, the FRF of the tool point is directly taken as $G(\omega)$. However; if the flexibility of the workpiece is considered, the FRF of the system is calculated by the addition of the tool point FRF and the workpiece FRF at the contact position [12, 13]:

$$\left[G(\omega)\right] = \left[G_{tool}(\omega) + G_{workpiece}(\omega)\right] \tag{1.2}$$

The tool point FRF can be obtained by analytical methods or by experimental techniques. Analytical methods to predict the dynamics of the spindle-tool holder-tool system have been developed in detail in recent studies by Ertürk et al. [14-17]. Experimental modal analysis can also be used to obtain the tool dynamics.

The effect of the workpiece dynamics to chatter is investigated by several researchers. Bravo et al. [12] and Thevenot et al. [18, 19] demonstrated that for thin-walled structures, part dynamics affects the stability. They proposed the three-dimensional stability lobe diagram, third dimension being the steps of the machining or the tool position. The stability lobe for the intermediate stages of the machining are plotted to obtain the 3D stability diagram. Le Lan et al. [20] used the finite element method to determine the stable depths of cut over a machining process and showed them on a color axis called stability map. A model considering the effect of part dynamics during milling was developed by Mañé et al. [21] and they optimized the productivity by controlling the spindle speed during machining. Weinert et al. [22] studied the five-axis milling process in time domain and modeled the workpiece by finite elements. The material removal effect has been introduced to chatter stability by Atlar et al. [13]. They modeled the workpiece as a beam and revealed the change of dynamics and therefore the stability as the workpiece is machined.

In this study, structural modification method is applied in order to take the effects of material removal into account. Structural modification is used to obtain the change in the dynamics of an original system if it is modified by a modifying structure. There are two types of structural modification problems: direct problem and inverse problem [23]. In the direct problem, the intention is to determine the dynamics of the structure after modification and the procedure is straightforward. The inverse problem, on the other hand, aims to determine the necessary modification to obtain a defined modified system.

In this work, part dynamics is required to be predicted during a machining cycle. The dynamics of the original and the modifying structures are known and that of the modified structure is sought, so the problem in hand is of direct type.

Direct structural modification, also named reanalysis, is practical to be used in design processes. Design alternatives with different modifications to an original structure may be too difficult to analyze with experiments and finite element methods. Using reanalysis, for a known original system dynamics, the design alternatives can easily be resolved and the dynamics of modified systems can be obtained.

Özgüven [24] developed an exact and general method for structural modifications using frequency response functions. The method is applicable even for cases with additional degrees of freedom due to modification. The input for the method is the FRFs of the original system and the dynamic properties of the modifying structure. The FRFs of the

modified structure are obtained as the output of the method. For machining stability analysis, the FRF of the workpiece at each step is required to be known, so the method mentioned is applicable, since it is FRF based.

Structural modification will be applied with additional degrees of freedom in this study. The workpiece will be modeled by finite element method as three-dimensional solids. The dynamic properties of the modifying structure include the mass and stiffness matrices of the material added. These matrices will be calculated during modification using the geometries of the elements in the added material. Mass and stiffness matrices of 3D linear brick elements are derived by applying the general procedure given by Cook et al. [25]. Numerical integration will be performed to calculate the integrals in the procedure. The sampling points for the 3D tetrahedral solid elements are taken from the book of Macneal [26].

1.3 Scope of the Thesis

The outline of the dissertation is given below:

In Chapter 2, the theoretical background of the study is presented. First, the structural modification technique used will be introduced and the theory of the method will be given briefly. Then, the modeling of two finite elements, the eight node hexahedral element and the ten-node tetrahedral element, will be shown.

In Chapter 3, the procedure of predicting the part dynamics by using the structural modification method will be given. The steps in the procedure

will be explained in detail. The procedure will be applied to parts with different geometries to show the prediction accuracy of the method employed.

In Chapter 4, the effects of part dynamics on machining stability will be examined for a case study in three axis machining. Machining stability analysis will be performed for different cutting strategies for the predicted part dynamics. The strategies will be compared for productivity.

In Chapter 5, machining stability analysis for a case study in five axis machining will be performed for predicted workpiece dynamics. Different strategies will be compared for productivity in five axis machining.

In the last chapter, the results will be discussed and suggestions for future work in the field will be given.

CHAPTER 2

THEORY

2.1 Structural Modification with Additional Degrees of Freedom

In this section, the structural modification method with additional degrees of freedom will be introduced. The formulation of the method employed will be given briefly and the implementation in Matlab will be presented.

2.1.1 Matrix Inversion Method

Matrix Inversion Method is an FRF based structural modification method developed by Özgüven [24]. Using the FRFs of the original system and the dynamic structural matrix of the modifying system, the FRFs of the modified system are calculated.

Two different formulations are given in this method. The first one is applicable for structural modification without adding new degrees of freedom. The second one is for the systems which have additional degrees of freedom due to the modification. In this work, structural modification with additional degrees of freedom is used, since without adding new nodes, it is not practical to model the material removal from the workpiece in the machining steps.

The formulation of the structural modification with additional degrees of freedom is given below. The equation of motion for a dynamic system can be written as:

$$[M]\{\ddot{x}\} + i[H]\{\dot{x}\} + [K]\{x\} = \{F\} \tag{2.1}$$

In the above equation; $[M]$, $[H]$ and $[K]$ denote the mass, structural damping and stiffness matrices of the system, respectively. $\{F\}$ and $\{x\}$ vectors are the generalized force and coordinate vectors. The response $\{x\}$ of the system to a harmonic force $\{F\}$ with frequency ω can be expressed as:

$$\{x\} = \left[[K] - \omega^2[M] + i[H]\right]^{-1}\{F\} \tag{2.2}$$

The receptance matrix, $[\alpha]$, is defined by:

$$[\alpha] = \left[[K] - \omega^2[M] + i[H]\right]^{-1} \tag{2.3}$$

A structural modification to the original structure may be represented by the modification matrices, $[\Delta M]$, $[\Delta H]$ and $[\Delta K]$. Dynamic structural modification matrix, $[D]$, can be written as:

$$[D] = [\Delta K] - \omega^2[\Delta M] + i[\Delta H] \tag{2.4}$$

The receptance matrix, $[\gamma]$, of the modified structure is in the form of:

$$[\gamma]=\left[[[K]+[\Delta K]]-\omega^2[[M]+[\Delta M]]+i[[H]+[\Delta H]]\right]^{-1} \tag{2.5}$$

The coordinates of the modified structure can be divided into three groups. The first group, (a), involves the unmodified coordinates of the original structure. The second group, (b), is the group of coordinates which are contained by both the original and the modifying structures. The coordinates in the third group, (c), are the ones which belong only to the modifying structure. Using this classification, equations (2.3) and (2.5) can be rewritten as follows:

$$[\alpha]^{-1}=\begin{bmatrix}\alpha_{aa} & \alpha_{ab}\\ \alpha_{ba} & \alpha_{bb}\end{bmatrix}^{-1}=[K]-\omega^2[M]+i[H] \tag{2.6}$$

$$\begin{bmatrix}\gamma_{aa} & \gamma_{ab} & \gamma_{ac}\\ \gamma_{ba} & \gamma_{bb} & \gamma_{bc}\\ \gamma_{ca} & \gamma_{cb} & \gamma_{cc}\end{bmatrix}^{-1}=\begin{bmatrix}[\alpha]^{-1} & 0\\ 0\ \ 0 & 0\end{bmatrix}+\begin{bmatrix}0 & 0 & 0\\ 0 & & \\ 0 & & [D]\end{bmatrix} \tag{2.7}$$

Note that in the above equations, α_{ij} and γ_{ij} are submatrices of $[\alpha]$ and $[\gamma]$, respectively. If equation (2.7) is pre-multiplied by

$$\begin{bmatrix}[\alpha] & 0\\ & 0\\ 0\ \ 0 & I\end{bmatrix}$$

and post-multiplied by $[\gamma]$, the following equation can be obtained:

$$\begin{bmatrix} [\alpha] & 0 \\ 0 \quad 0 & I \end{bmatrix} = \begin{bmatrix} I & 0 & 0 \\ 0 & I & 0 \\ 0 & 0 & I \end{bmatrix} [\gamma] + \begin{bmatrix} 0 & [\alpha_{ab} \quad 0] \bullet [D] \\ 0 & \begin{bmatrix} \alpha_{bb} & 0 \\ 0 & I \end{bmatrix} \bullet [D] \end{bmatrix} [\gamma] \tag{2.8}$$

Equation (2.8) can be operated to obtain the following equation:

$$\begin{bmatrix} \alpha_{aa} & \alpha_{ab} & 0 \\ \alpha_{ba} & \alpha_{bb} & 0 \\ 0 & 0 & I \end{bmatrix} = \begin{bmatrix} \gamma_{aa} & \gamma_{ab} & \gamma_{ac} \\ \gamma_{ba} & \gamma_{bb} & \gamma_{bc} \\ 0 & 0 & 0 \end{bmatrix} + \begin{bmatrix} [\alpha_{ab} \quad 0] \bullet [D] \begin{bmatrix} \gamma_{ba} \\ \gamma_{ca} \end{bmatrix} & [\alpha_{ab} \quad 0] \bullet [D] \begin{bmatrix} \gamma_{bb} & \gamma_{bc} \\ \gamma_{cb} & \gamma_{cc} \end{bmatrix} \\ \begin{bmatrix} \alpha_{bb} & 0 \\ 0 & I \end{bmatrix} \bullet [D] \begin{bmatrix} \gamma_{ba} \\ \gamma_{ca} \end{bmatrix} & \begin{bmatrix} \alpha_{bb} & 0 \\ 0 & I \end{bmatrix} \bullet [D] \begin{bmatrix} \gamma_{bb} & \gamma_{bc} \\ \gamma_{cb} & \gamma_{cc} \end{bmatrix} \end{bmatrix} \tag{2.9}$$

The relations (2.10) and (2.11) are used to obtain the equations (2.12) to (2.15) from (2.9):

$$\begin{bmatrix} I & 0 \\ 0 & 0 \end{bmatrix} \begin{bmatrix} \gamma_{bb} & \gamma_{bc} \\ \gamma_{cb} & \gamma_{cc} \end{bmatrix} = \begin{bmatrix} \gamma_{bb} & \gamma_{bc} \\ 0 & 0 \end{bmatrix} \tag{2.10}$$

$$\begin{bmatrix} I & 0 \\ 0 & 0 \end{bmatrix} \begin{bmatrix} \gamma_{ba} \\ \gamma_{ca} \end{bmatrix} = \begin{bmatrix} \gamma_{ba} \\ 0 \end{bmatrix} \tag{2.11}$$

$$\left(\begin{bmatrix} I & 0 \\ 0 & 0 \end{bmatrix} + \begin{bmatrix} \alpha_{bb} & 0 \\ 0 & I \end{bmatrix} \bullet [D] \right) \begin{bmatrix} \gamma_{ba} \\ \gamma_{ca} \end{bmatrix} = \begin{bmatrix} \alpha_{ba} \\ 0 \end{bmatrix} \tag{2.12}$$

$$\left(\begin{bmatrix} I & 0 \\ 0 & 0 \end{bmatrix} + \begin{bmatrix} \alpha_{bb} & 0 \\ 0 & I \end{bmatrix} \bullet [D] \right) \begin{bmatrix} \gamma_{bb} & \gamma_{bc} \\ \gamma_{cb} & \gamma_{cc} \end{bmatrix} = \begin{bmatrix} \alpha_{bb} & 0 \\ 0 & I \end{bmatrix} \tag{2.13}$$

$$[\gamma_{aa}] + [\alpha_{ab} \quad 0][D] \begin{bmatrix} \gamma_{ba} \\ \gamma_{ca} \end{bmatrix} = [\alpha_{aa}] \tag{2.14}$$

$$\begin{bmatrix}\gamma_{ab} & \gamma_{ac}\end{bmatrix}+\begin{bmatrix}\alpha_{ab} & 0\end{bmatrix}[D]\begin{bmatrix}\gamma_{bb} & \gamma_{bc}\\ \gamma_{cb} & \gamma_{cc}\end{bmatrix}=\begin{bmatrix}\alpha_{ab} & 0\end{bmatrix} \tag{2.15}$$

The parts of the receptance matrix of the modified structure are obtained as:

$$\begin{bmatrix}\gamma_{ba}\\ \gamma_{ca}\end{bmatrix}=\left[\begin{bmatrix}I & 0\\ 0 & 0\end{bmatrix}+\begin{bmatrix}\alpha_{bb} & 0\\ 0 & I\end{bmatrix}\cdot[D]\right]^{-1}\begin{bmatrix}\alpha_{ba}\\ 0\end{bmatrix} \tag{2.16}$$

$$\begin{bmatrix}\gamma_{bb} & \gamma_{bc}\\ \gamma_{cb} & \gamma_{cc}\end{bmatrix}=\left[\begin{bmatrix}I & 0\\ 0 & 0\end{bmatrix}+\begin{bmatrix}\alpha_{bb} & 0\\ 0 & I\end{bmatrix}\cdot[D]\right]^{-1}\begin{bmatrix}\alpha_{bb} & 0\\ 0 & I\end{bmatrix} \tag{2.17}$$

$$[\gamma_{aa}]=[\alpha_{aa}]-[\alpha_{ab} \quad \vdots \quad 0][D]\begin{bmatrix}\gamma_{ba}\\ \gamma_{ca}\end{bmatrix} \tag{2.18}$$

$$[\gamma_{ab} \quad \vdots \quad \gamma_{ac}]=[\alpha_{ab} \quad \vdots \quad 0]\left[[I]-[D]\begin{bmatrix}\gamma_{bb} & \gamma_{bc}\\ \gamma_{cb} & \gamma_{cc}\end{bmatrix}\right] \tag{2.19}$$

In the above formulation, only a single matrix inversion is necessary. The order of this matrix is equal to the degree of freedom of the modifying structure and it is generally much less than the degree of freedom of the modified structure. Note that the computation effort for matrix inversion becomes extremely high if the size of the matrix increases. Therefore, the proposed method brings computational efficiency for local modifications.

2.1.2 Implementation of the Method

The formulation described above is implemented in the software Matlab using two functions. The first function is the organization function. In this function, the matrices $[\alpha]$ and $[D]$, and the node numbers relevant to the

degrees of freedom of these matrices are taken as input. The intersecting nodes in the two node vectors are found. The elements of the $[\alpha]$ matrix for the coordinates on the intersecting nodes must be on the lowermost rows and rightmost columns. Similarly, the elements related with the intersecting coordinates of the $[D]$ matrix must be on the topmost rows and leftmost columns. The matrices are reorganized to be ready for the matrix operations. The second function, i.e. the calculation function, directly applies the equations (2.16) through (2.19) and calculates the components of the FRF, $[\gamma]$, of the modified structure.

2.2 Finite Element Modeling of Basic Solid Elements

This section presents the modeling of two solid finite elements, the eight-node hexahedral element and the ten-node tetrahedral element. The stiffness and mass matrices of these elements will be obtained as the outcome of the modeling. These matrices will be used in the structural modification procedure which represents the machining process of three-dimensional workpiece.

2.2.1 Eight-node Hexahedral Linear Solid Element

The element is also known as eight-node brick element. The stiffness and mass matrices of an eight-node linear solid element will be obtained in this section. The degree of freedom of the element is 24, with three orthogonal translational displacement freedoms at each of the eight nodes.

The stiffness matrix of a three-dimensional structure is given as [25]:

$$[K] = \int_V [B]^T [E][B] dV \tag{2.20}$$

Here, $[B]$ is the strain-displacement relation matrix for 3D elastic body and $[E]$ is the elasticity matrix. The elasticity matrix of an isotropic element in 3D can be written as:

$$[E] = E' \begin{bmatrix} (1-\nu) & \nu & \nu & 0 & 0 & 0 \\ \nu & (1-\nu) & \nu & 0 & 0 & 0 \\ \nu & \nu & (1-\nu) & 0 & 0 & 0 \\ 0 & 0 & 0 & \frac{1-2\nu}{2} & 0 & 0 \\ 0 & 0 & 0 & 0 & \frac{1-2\nu}{2} & 0 \\ 0 & 0 & 0 & 0 & 0 & \frac{1-2\nu}{2} \end{bmatrix} \tag{2.21}$$

where

$$E' = \frac{E}{(1+\nu)(1-2\nu)} \tag{2.22}$$

E and ν are the modulus of elasticity and the Poisson's ratio, respectively. The strains, $\{\varepsilon\}$, and the displacements of the structure, $\{\Delta\}$, are related to each other with the strain-displacement matrix $[B]$ as:

$$\{\varepsilon\} = [B]\{\Delta\} \tag{2.23}$$

The strain matrix in 3D is in the form of:

$$\{\varepsilon\} = \begin{Bmatrix} \varepsilon_x \\ \varepsilon_y \\ \varepsilon_z \\ \gamma_{xy} \\ \gamma_{yz} \\ \gamma_{zx} \end{Bmatrix} \tag{2.24}$$

The displacement matrix in 3D can be written as:

$$\{\Delta\} = \begin{Bmatrix} u \\ v \\ w \end{Bmatrix} \tag{2.25}$$

where u, v and w are the displacements in x, y and z directions, respectively. The strain-displacement matrix has the form:

$$[B]^T = \begin{bmatrix} \frac{\partial}{\partial x} & 0 & 0 & \frac{\partial}{\partial y} & 0 & \frac{\partial}{\partial z} \\ 0 & \frac{\partial}{\partial y} & 0 & \frac{\partial}{\partial x} & \frac{\partial}{\partial z} & 0 \\ 0 & 0 & \frac{\partial}{\partial z} & 0 & \frac{\partial}{\partial y} & \frac{\partial}{\partial x} \end{bmatrix} \tag{2.26}$$

The displacement of a point on the element can be expressed using the shape functions and the nodal displacements. Using the same shape functions in three directions, the displacement vector can be written as:

$$\{\Delta\} = \begin{Bmatrix} \sum_{i=1}^{8} N_i u_i \\ \sum_{i=1}^{8} N_i v_i \\ \sum_{i=1}^{8} N_i w_i \end{Bmatrix} = \begin{bmatrix} N_1 & 0 & 0 & N_2 & \dots & N_8 & 0 & 0 \\ 0 & N_1 & 0 & 0 & N_2 & \dots & N_8 & 0 \\ 0 & 0 & N_1 & 0 & 0 & N_2 & \dots & N_8 \end{bmatrix} \{\delta\} \tag{2.27}$$

where $\left[\delta^T\right] = \left(u_1, v_1, w_1, \dots, u_8, v_8, w_8\right)$. From equations (2.23), (2.24), (2.26) and (2.27) the matrix $[B]$ can be expressed as:

$$[B] = \begin{bmatrix} \frac{\partial N_1}{\partial x} & 0 & 0 & \frac{\partial N_2}{\partial x} & \dots & \frac{\partial N_8}{\partial x} & 0 & 0 \\ 0 & \frac{\partial N_1}{\partial y} & 0 & 0 & \frac{\partial N_2}{\partial y} & \dots & \frac{\partial N_8}{\partial y} & 0 \\ 0 & 0 & \frac{\partial N_1}{\partial z} & 0 & 0 & \frac{\partial N_2}{\partial z} & \dots & \frac{\partial N_8}{\partial z} \\ \frac{\partial N_1}{\partial y} & \frac{\partial N_1}{\partial x} & 0 & \dots & 0 & \frac{\partial N_8}{\partial y} & \frac{\partial N_8}{\partial x} & 0 \\ 0 & \frac{\partial N_1}{\partial z} & \frac{\partial N_1}{\partial y} & 0 & \dots & 0 & \frac{\partial N_8}{\partial z} & \frac{\partial N_8}{\partial y} \\ \frac{\partial N_1}{\partial z} & 0 & \frac{\partial N_1}{\partial x} & \frac{\partial N_2}{\partial z} & \dots & \frac{\partial N_8}{\partial z} & 0 & \frac{\partial N_8}{\partial x} \end{bmatrix} \tag{2.28}$$

The 3D isoparametric element, shown in Figure 2.1 is used in the formulation. This element is superior to be applied to different geometry. The edge lengths and the angles between the edges in the element can be different.

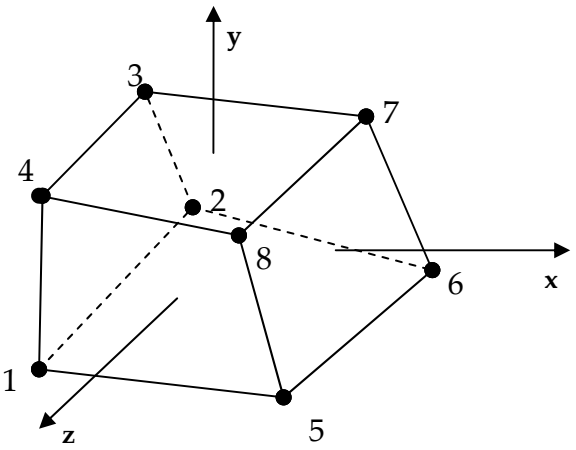

Figure 2.1. 3D isoparametric solid element

Using the global coordinate system, it is very difficult to model and analyze the elements with irregular geometry. To simplify the geometry and the analysis, the natural coordinate system is introduced. The 3D solid element in the natural coordinates is shown in Figure 2.2.

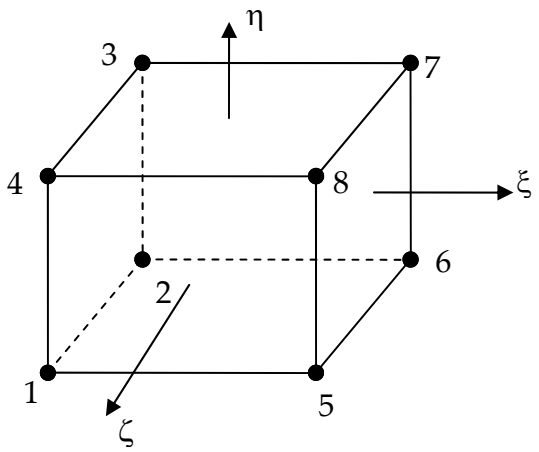

Figure 2.2. The 3D solid element in natural coordinates

The element matrices are obtained using the natural coordinates. Numerical integration is used to calculate the volume integrals and it is easy to perform numerical integration in natural coordinates.

For isoparametric elements, the relation between the global and natural coordinates is given as follows:

$$x=\sum_{i=1}^{8} x_i N_i(\xi,\eta,\zeta),\ \ y=\sum_{i=1}^{8} y_i N_i(\xi,\eta,\zeta),\ \ z=\sum_{i=1}^{8} z_i N_i(\xi,\eta,\zeta) \tag{2.29}$$

where (x_i, y_i, z_i) are the nodal coordinates in the global coordinate system. The same shape functions N_i are used to express both the coordinates and the displacements in the isoparametric element. The shape functions in the natural coordinates $-1 \le \xi,\eta,\zeta \le 1$ are:

$$\begin{aligned}
N_1 &= \frac{1}{8}(1-\xi)(1-\eta)(1+\zeta)\\
N_2 &= \frac{1}{8}(1-\xi)(1-\eta)(1-\zeta)\\
N_3 &= \frac{1}{8}(1-\xi)(1+\eta)(1-\zeta)\\
N_4 &= \frac{1}{8}(1-\xi)(1+\eta)(1+\zeta)\\
N_5 &= \frac{1}{8}(1+\xi)(1-\eta)(1+\zeta)\\
N_6 &= \frac{1}{8}(1+\xi)(1-\eta)(1-\zeta)\\
N_7 &= \frac{1}{8}(1+\xi)(1+\eta)(1-\zeta)\\
N_8 &= \frac{1}{8}(1+\xi)(1+\eta)(1+\zeta)
\end{aligned} \tag{2.30}$$

The value of the shape function N_i is unity at the i^{th} node and zero at the other nodes of the element. The variables of the integral of the stiffness matrix can be changed to natural coordinates as:

$$[K] = \int_V [B]^T [E][B]\, dxdydz = \int_{-1}^{1}\int_{-1}^{1}\int_{-1}^{1} [B]^T [E][B] \det[J]\, d\xi d\eta d\zeta \tag{2.31}$$

Here, $[J]$ is the Jacobian of the transformation between the global and natural coordinates. The determinant of the Jacobian matrix in the integral can be considered as a factor that scales the volumes in two coordinate systems. To procure $[B]$ matrix, the derivatives of the shape functions with respect to the global coordinates ($\partial N_i / \partial x$, etc.) are required. The transformation between the coordinate systems is given as follows:

$$\begin{Bmatrix} \frac{\partial}{\partial \xi} \\ \frac{\partial}{\partial \eta} \\ \frac{\partial}{\partial \zeta} \end{Bmatrix} = [J] \begin{Bmatrix} \frac{\partial}{\partial x} \\ \frac{\partial}{\partial y} \\ \frac{\partial}{\partial z} \end{Bmatrix} \tag{2.32}$$

The elements of the Jacobian matrix are:

$$[J] = \begin{bmatrix} \frac{\partial x}{\partial \xi} & \frac{\partial y}{\partial \xi} & \frac{\partial z}{\partial \xi} \\ \frac{\partial x}{\partial \eta} & \frac{\partial y}{\partial \eta} & \frac{\partial z}{\partial \eta} \\ \frac{\partial x}{\partial \zeta} & \frac{\partial y}{\partial \zeta} & \frac{\partial z}{\partial \zeta} \end{bmatrix} \tag{2.33}$$

Using equation (2.29), the derivatives of the global coordinates with respect to the natural ones can be obtained:

$$\begin{aligned}
&\frac{\partial x}{\partial \xi}=\sum_{i=1}^{8} x_i \frac{\partial N_i}{\partial \xi}, \quad \frac{\partial y}{\partial \xi}=\sum_{i=1}^{8} y_i \frac{\partial N_i}{\partial \xi}, \quad \frac{\partial z}{\partial \xi}=\sum_{i=1}^{8} z_i \frac{\partial N_i}{\partial \xi} \\
&\frac{\partial x}{\partial \eta}=\sum_{i=1}^{8} x_i \frac{\partial N_i}{\partial \eta}, \quad \frac{\partial y}{\partial \eta}=\sum_{i=1}^{8} y_i \frac{\partial N_i}{\partial \eta}, \quad \frac{\partial z}{\partial \eta}=\sum_{i=1}^{8} z_i \frac{\partial N_i}{\partial \eta} \\
&\frac{\partial x}{\partial \zeta}=\sum_{i=1}^{8} x_i \frac{\partial N_i}{\partial \zeta}, \quad \frac{\partial y}{\partial \zeta}=\sum_{i=1}^{8} y_i \frac{\partial N_i}{\partial \zeta}, \quad \frac{\partial z}{\partial \zeta}=\sum_{i=1}^{8} z_i \frac{\partial N_i}{\partial \zeta}
\end{aligned} \tag{2.34}$$

Inverting equation (2.32), the following equation can be obtained:

$$\begin{Bmatrix} \frac{\partial}{\partial x} \\ \frac{\partial}{\partial y} \\ \frac{\partial}{\partial z} \end{Bmatrix} = [L] \begin{Bmatrix} \frac{\partial}{\partial \xi} \\ \frac{\partial}{\partial \eta} \\ \frac{\partial}{\partial \zeta} \end{Bmatrix} \tag{2.35}$$

The derivatives of the shape functions in the natural coordinates can be obtained analytically for N_1 as follows:

$$\frac{\partial N_1}{\partial \xi}=-\frac{1}{8}(1-\eta)(1+\zeta), \frac{\partial N_1}{\partial \eta}=-\frac{1}{8}(1-\xi)(1+\zeta), \frac{\partial N_1}{\partial \zeta}=\frac{1}{8}(1-\xi)(1-\eta) \tag{2.36}$$

The derivatives for the other shape functions can be written in the similar form. The matrix $[J]$, however, has to be inverted numerically. The integration in equation (2.31) can be calculated to obtain the stiffness matrix of the eight node hexahedral element. The Gauss quadrature is used as the numerical integration method:

$$\int_{-1}^{1}\int_{-1}^{1}\int_{-1}^{1}[B]^T[E][B]\det[J]d\xi d\eta d\zeta = \\ =\sum_{i=1}^{m}\sum_{i=1}^{m}\sum_{i=1}^{m}H_iH_jH_k\left([B]^T[E][B]\det[J]\right)_{\xi_i\eta_i\zeta_i} \tag{2.37}$$

where m is the number of sampling points, H_i are the weighting factors for the i^{th} point and ξ_i,η_i,ζ_i are the coordinates of the sampling point. $[B]$ and $\det[J]$ have to be calculated at each sampling point. Two points integration in each direction is necessary for convergence. The reason is that the determinant of the $[J]$ matrix has quadratic terms and therefore the order of the integrand is 2, assuming small element sizes and so constant $[B]$ matrix. 2x2x2 integration is performed for three-dimensional integration. The integration points are $P_i\left(\pm1/\sqrt{3},\pm1/\sqrt{3},\pm1/\sqrt{3}\right)$ and the weighting factors are $H_i=1$. The stiffness matrix can be obtained by numerical integration at the eight points described.

Since linear shape functions are used in the formulation, parasitic shear occurs in the element modeled. This causes the element be too stiff in bending. This problem can be surpassed by adding the missing modes as internal freedoms to append quadrilateral terms to the displacement expression [25]:

$$\begin{aligned} u &= \sum_{i=1}^{8}N_iu_i+\left(1-\xi^2\right)a_1+\left(1-\eta^2\right)a_2+\left(1-\zeta^2\right)a_3 \\ v &= \sum_{i=1}^{8}N_iv_i+\left(1-\xi^2\right)a_4+\left(1-\eta^2\right)a_5+\left(1-\zeta^2\right)a_6 \\ w &= \sum_{i=1}^{8}N_iw_i+\left(1-\xi^2\right)a_7+\left(1-\eta^2\right)a_8+\left(1-\zeta^2\right)a_9 \end{aligned} \tag{2.38}$$

where a_i are the nodeless degrees of freedom. With the inclusion of internal freedoms, the elemental equation can be written as:

$$\begin{bmatrix} [K_{ee}] & [K_{ea}] \\ [K_{ae}] & [K_{aa}] \end{bmatrix} \begin{Bmatrix} \{\delta\} \\ \{a\} \end{Bmatrix} = \begin{Bmatrix} \{Q\}_{(24)} \\ \{0\}_{(9)} \end{Bmatrix} \tag{2.39}$$

Here, $\{a\}$ is the nodeless degrees of freedom vector with nine elements, and the matrices $[K_{ea}]$, $[K_{ae}]$ and $[K_{aa}]$ contain quadratic terms. Note that $\{\delta\}$ is the nodal displacement vector with 24 elements. Since $\{u\}$ vector has now 33 terms, the size of $[B]$ matrix is 6×33. Using static condensation [25], the nodeless degrees of freedom can be eliminated to have the elemental equation in the form:

$$[K'_{ee}]\{\delta\} = \{Q\} \tag{2.40}$$

where $[K'_{ee}]$ is the new elemental stiffness matrix and can be obtained by:

$$[K'_{ee}] = \left[[K_{ee}] - [K_{ea}][K_{aa}]^{-1}[K_{ae}] \right] \tag{2.41}$$

The new element was tested for different geometries in which the edges are in orthogonal directions and observed to have the same stiffness matrix with the one obtained from the finite element program Ansys, which verifies the modeling of the finite element.

The mass matrix of a three-dimensional structure is given by [25]:

$$[M] = \int_V \rho [N]^T [N] dV \tag{2.42}$$

where ρ is the mass density and $[N]$ is the shape function matrix. As performed in stiffness matrix calculation, Gauss quadrature with eight points over the volume can be used to obtain the elemental mass matrix:

$$[M] = \int_{-1}^{1}\int_{-1}^{1}\int_{-1}^{1} \rho [N]^T [N] \det[J] d\xi d\eta d\zeta = \sum_{i=1}^{8} \left(\rho [N]^T [N] \det[J] \right)_{P_i} \tag{2.43}$$

The mass matrix of the element model using the described formulation is the same as the mass matrix of the same element modeled in Ansys.

2.2.2 Ten-node Tetrahedral Linear Solid Element

The degree of freedom of the element is 30, with three orthogonal displacement freedoms at each of the ten nodes (Figure 2.3). The procedure applied to model this element is similar to the one for the eight-node brick element. Equations (2.20 - 2.26) are valid for the ten-node tetrahedral element as well.

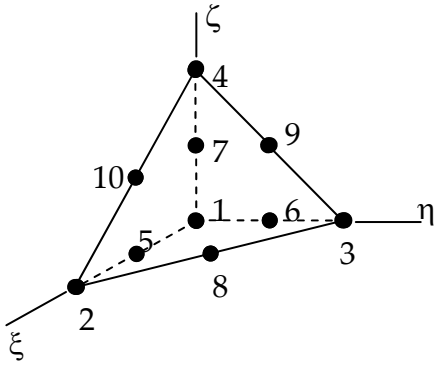

Figure 2.3. Ten-node tetrahedral solid element in the natural coordinates

Using the 30 degrees of freedom, $\{\delta^T\} = (u_1, v_1, w_1, \ldots, u_{10}, v_{10}, w_{10})$, the displacement vector can be written as:

$$\{\Delta\} = \begin{Bmatrix} \sum_{i=1}^{10} N_i u_i \\ \sum_{i=1}^{10} N_i v_i \\ \sum_{i=1}^{10} N_i w_i \end{Bmatrix} = \begin{bmatrix} N_1 & 0 & 0 & N_2 & \ldots & N_{10} & 0 & 0 \\ 0 & N_1 & 0 & 0 & N_2 & \ldots & N_{10} & 0 \\ 0 & 0 & N_1 & 0 & 0 & N_2 & \ldots & N_{10} \end{bmatrix} \{\delta\} \tag{2.44}$$

Equations (2.23), (2.24), (2.26) and (2.44) lead to the strain-displacement matrix:

$$[B] = \begin{bmatrix} \frac{\partial N_1}{\partial x} & 0 & 0 & \frac{\partial N_2}{\partial x} & \ldots & \frac{\partial N_{10}}{\partial x} & 0 & 0 \\ 0 & \frac{\partial N_1}{\partial y} & 0 & 0 & \frac{\partial N_2}{\partial y} & \ldots & \frac{\partial N_{10}}{\partial y} & 0 \\ 0 & 0 & \frac{\partial N_1}{\partial z} & 0 & 0 & \frac{\partial N_2}{\partial z} & \ldots & \frac{\partial N_{10}}{\partial z} \\ \frac{\partial N_1}{\partial y} & \frac{\partial N_1}{\partial x} & 0 & \ldots & 0 & \frac{\partial N_{10}}{\partial y} & \frac{\partial N_{10}}{\partial x} & 0 \\ 0 & \frac{\partial N_1}{\partial z} & \frac{\partial N_1}{\partial y} & 0 & \ldots & 0 & \frac{\partial N_{10}}{\partial z} & \frac{\partial N_{10}}{\partial y} \\ \frac{\partial N_1}{\partial z} & 0 & \frac{\partial N_1}{\partial x} & \frac{\partial N_2}{\partial z} & \ldots & \frac{\partial N_{10}}{\partial z} & 0 & \frac{\partial N_{10}}{\partial x} \end{bmatrix} \tag{2.45}$$

The relation between the global and natural coordinates is the same as in equation (2.29), with the exception that there are ten nodes at present:

$$x=\sum_{i=1}^{10} x_i N_i(\xi,\eta,\zeta),\quad y=\sum_{i=1}^{10} y_i N_i(\xi,\eta,\zeta),\quad z=\sum_{i=1}^{10} z_i N_i(\xi,\eta,\zeta) \tag{2.46}$$

The shape functions for the tetrahedral element are:

$$\begin{aligned}
N_1 &= (1-\xi-\eta-\zeta)(1-2\xi-2\eta-2\zeta)\\
N_2 &= \xi(1-2\xi)\\
N_3 &= \eta(1-2\eta)\\
N_4 &= \zeta(1-2\zeta)\\
N_5 &= 4\xi(1-\xi-\eta-\zeta)\\
N_6 &= 4\eta(1-\xi-\eta-\zeta)\\
N_7 &= 4\zeta(1-\xi-\eta-\zeta)\\
N_8 &= 4\xi\eta\\
N_9 &= 4\eta\zeta\\
N_{10} &= 4\zeta\xi
\end{aligned} \tag{2.47}$$

The definition of the Jacobian is the same as in hexahedral element. The derivatives of the shape functions in the natural coordinates can again be taken analytically. Numerical integration will be applied to calculate the integral of the stiffness matrix. Macneal [26] suggested four-point integration to approximate the volume integral of the tetrahedral element.

Table 2.1. Integration points for the tetrahedral element [26]

ξ	η	ζ	Weight
α	β	β	1/24
β	α	β	1/24
β	β	α	1/24
β	β	β	1/24

where $\alpha = \left(5 + 3\sqrt{5}\right)/20 = 0.58541020$ and $\beta = \left(5 - \sqrt{5}\right)/20 = 0.13819660$.

The stiffness matrix of the tetrahedral element is calculated with the procedure described. It is observed that the calculated stiffness matrix for the tetrahedral element is the same as the stiffness matrix of the element modeled in Ansys. Similar procedure is followed to obtain the mass matrix of the element.

CHAPTER 3

THE PROCEDURE OF PREDICTING THE WORKPIECE DYNAMICS BY STRUCTURAL MODIFICATION

In this chapter, the algorithm of the workpiece dynamics prediction procedure developed and the application of this procedure to case studies will be presented. The computer programs used in the procedure are Ansys and Matlab. The machined workpiece is modeled with Ansys in order to obtain the dynamics of the workpiece for the final state of machining. Part dynamics at different stages of the machining is predicted by using Matlab. The procedure can be divided into three steps as:

- Geometric and finite element modeling
- Modal analysis and FRF extraction
- Structural modification and FRF prediction

The programming for the implementation of the method built up will be explained thoroughly.

3.1 Geometric and Finite Element Modeling of the Workpiece

The geometry of the workpiece is an input for the procedure. Part geometry must be defined for each stage where the dynamics is required to be predicted. Each volume removed between two successive stages is modeled

separately. The geometry of the workpiece can be modeled by using a CAD software or it may be modeled on Ansys.

All the volumes obtained in geometric modeling are glued in Ansys. Gluing the volumes provides rigid coupling between them. At the same time, the stages of the dynamic prediction are obtained as intermediate steps of the machining procedure. The unmachined model is meshed using three-dimensional solid elements. The data obtained by meshing are saved to be used in the following steps. These data include the element numbers on each volume, the node numbers on each element and the coordinates of each node.

3.2 Modal Analysis and FRF Extraction for the Initial Model

Modal analysis is performed for the machined workpiece geometry. The natural frequencies and the corresponding mode shapes are extracted and saved to be used in the calculation of the FRF of the machined workpiece.

The data obtained from the modal analysis are used to calculate the FRF of the machined geometry. The elements of the FRF, α_{ij}, can be written in terms of the natural frequencies, ω_r, and the mode shapes, $\{\phi^r\}$, as in the following equation:

$$\alpha_{ij} = \sum_{r=1}^{n} \frac{\{\phi_i^r\}\{\phi_j^r\}}{\omega_r^2 - \omega^2 + i\gamma_r\omega_r^2} \tag{3.1}$$

where ω is the frequency for which the elements of the FRF are calculated and γ_r is the damping coefficient of the r^{th} mode.

While calculating the FRF, some degrees of freedom can be considered as redundant degrees of freedom. If no more modification is to be applied on a degree of freedom, and also the dynamics about it is not required to be known, then it is not necessary to keep the element of the FRF matrix for this degree of freedom. For the initial state of the procedure, i.e. for the machined geometry, there will not be any modification on the degrees of freedom which are not common with the volumes machined. If it is not necessary to know the dynamics of these degrees of freedom for the machining stability analysis, the elements of the FRF related to these degrees of freedom are redundant.

3.3 Prediction of the Workpiece Dynamics at Different Machining Stages by Structural Modification

Structural modification is implemented in the software Matlab. The details of the method are given in Chapter 2. The data related with the machining cycle have been obtained from Ansys and saved in the previous steps. These data are the inputs for this step. The volumes removed during machining are added to the machined geometry, in a reverse order. Following the procedure presented in Chapter 2, the element matrices are obtained in Matlab by using the material properties and the geometry of the element.

For each volume, the elements can be added one by one, or as a group. The computation time depends on the number of elements added at each step. For lower number of elements per addition, more modification steps are required; hence the number of computation is higher. If the number of elements added at each step is increased, the number of computation decreases. However, as the number of elements added increases, the size of addition matrices increases. In the structural modification method used, the dynamic matrix of the addition element is inverted. The time for inversion and also the time for assembling the dynamics matrix become important as the size of the addition matrices increases. To minimize the computation time, for a frequency value, the structural modification procedure is applied for different number of elements added at each step. For the whole frequency range, the number of elements that gives the minimum computation time is used.

3.4 Case Studies

The procedure described above is applied to different geometries. The details of the geometries and the results of the procedure are given below.

3.4.1 Geometry 1

The first geometry is a simple one. The initial geometry shown in Figure 3.1 is a cube of sides 5 *mm* each and it is modeled in Ansys. An identical cube is added as modification from one side.

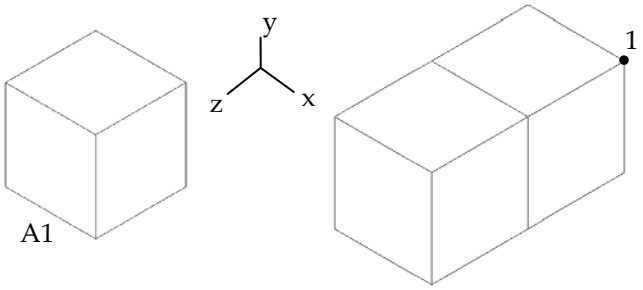

Figure 3.1. Initial and modified structures for geometry 1

Ten-node tetrahedral elements are used to mesh the geometry. The meshes of the models are given in Figure 3.2.

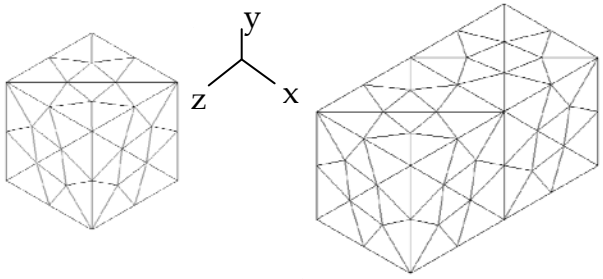

Figure 3.2. Mesh model of geometry 1.

The details of the model are listed in Table 3.1.

Table 3.1. Details about geometry 1

Modulus of elasticity (GPa)	200
Poisson's ratio	0.3
Density (kg/m^3)	7800
Number of nodes	425
DOF of initial model	582
Number of elements added	100

The initial cube is fixed from one of its faces (A1 in Figure 3.1). Modal analysis is performed for this model in Ansys and the outputs of the modal analysis are saved to be used in FRF extraction. The FRFs of the initial model are extracted in Matlab for different frequencies, and the elements of the second cube are added to these FRFs as modification. The model with two cubes is also analyzed in Ansys and the first two natural frequencies for this model are determined to be 35751 and 35761 *Hz*. The modification procedure is applied in a frequency range near these two frequencies. The FRF for the displacement in y-direction due to the force in y-direction of node 1 (Figure 3.1), obtained by modal analysis and predicted by the developed procedure are plotted in Figure 3.3.

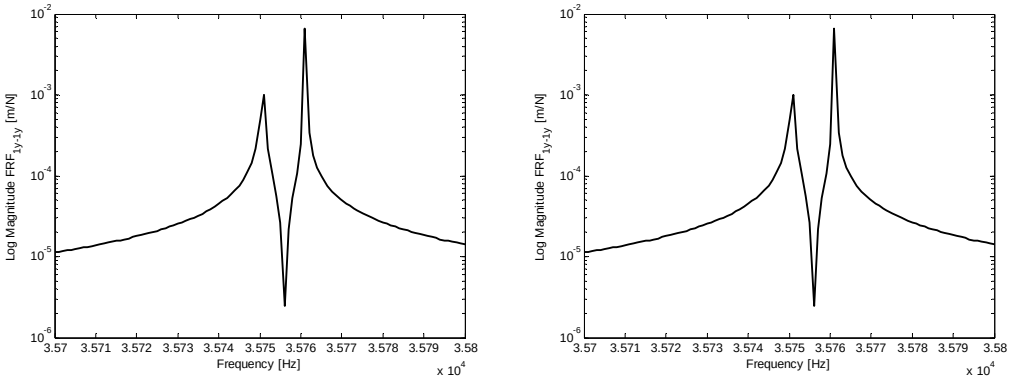

Figure 3.3. FRF plots for geometry 1; left plot: predicted by the developed method, right plot: analyzed in Ansys

It can be concluded that the FRF predicted by the method developed is the same as the FRF obtained by modal analysis.

3.4.2 Geometry 2

The second case study is the application of the method to a previous work. Atlar et al. [13] analyzed a workpiece modeled as a beam to show the change in the workpiece FRF during machining. They used structural modification without additional degrees of freedom to obtain the part dynamics through the machining process. In the current study, the same workpiece is modeled using three-dimensional solid elements, and structural modification with additional degrees of freedom is applied to predict the FRFs of the part in the intermediate steps.

The geometry of the workpiece is shown in Figure 3.4. The dimensions in the figure are in *mm*. The material is steel with the following material properties, 200 *GPa* Young's modulus, 0.3 Poisson's ratio and 7800 kg/m^3 density. The boundary conditions are fixed-free. The finite element analysis is performed by using the FE program MSC. Marc Mentat.

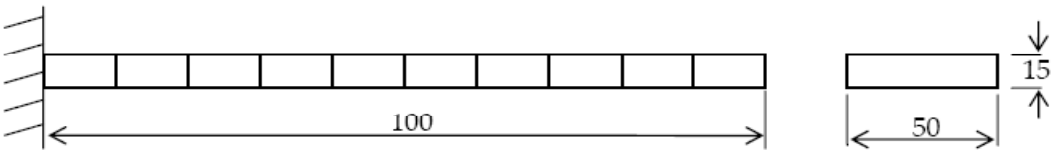

Figure 3.4. Beam model studied by Atlar et al. [13]

The thickness of the beam is 15 *mm* initially and it is decreased to 10 *mm*, 5 *mm* and 3 *mm* in the roughing, semi-finishing and finishing cuts, respectively. A coding convention is proposed to indicate the stage of machining. B19, for instance, denotes the 9^{th} step of the 1^{st} cut (roughing

cut). The FRFs of the workpiece at intermediate stages were calculated, and the ones for the steps shown in Figure 3.5 were plotted in Figure 3.6.

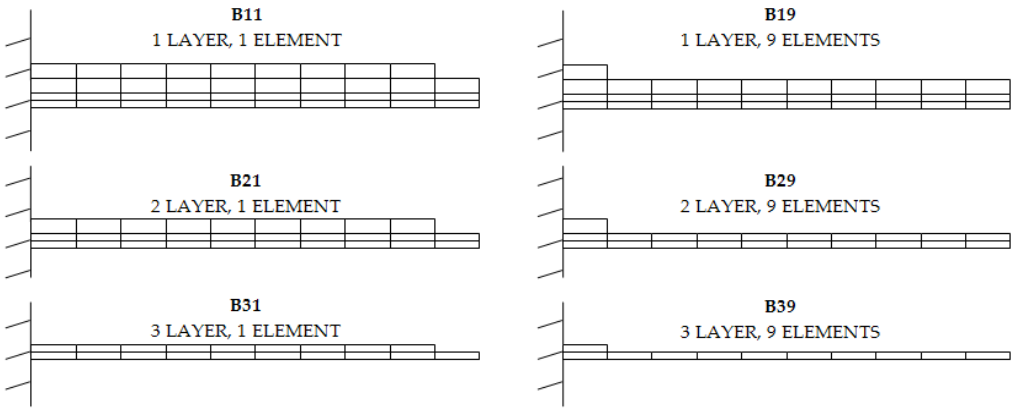

Figure 3.5. Beam models of 1st, 2nd and 3rd cuts at the end of, 1st (left) and 9th (right) steps [13].

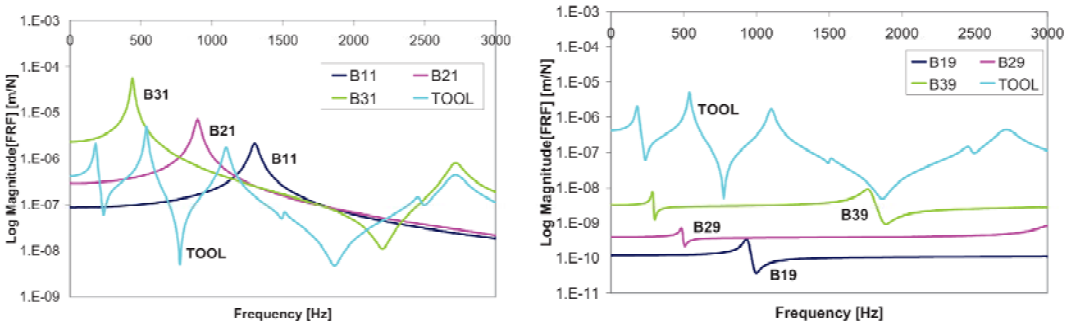

Figure 3.6. FRFs of the workpiece and the tool for the stages shown in Figure 3.5 [13]

Figure 3.6 is taken from the study of Atlar et al. [13]. The plots include the tool point FRF of the spindle-tool holder-tool system used in the machining stability analysis.

The model of the same geometry meshed by brick solid elements, and the steps of the machining are shown in Figure 3.8. Ansys is used as the finite element program. Table 3.2 presents the details of the model.

Table 3.2. Details about geometry 2

Number of nodes	220
Dof of initial model	240
Number of elements added	90

The predicted FRFs of the workpiece are plotted in Figure 3.7, for the nodes shown in Figure 3.8.

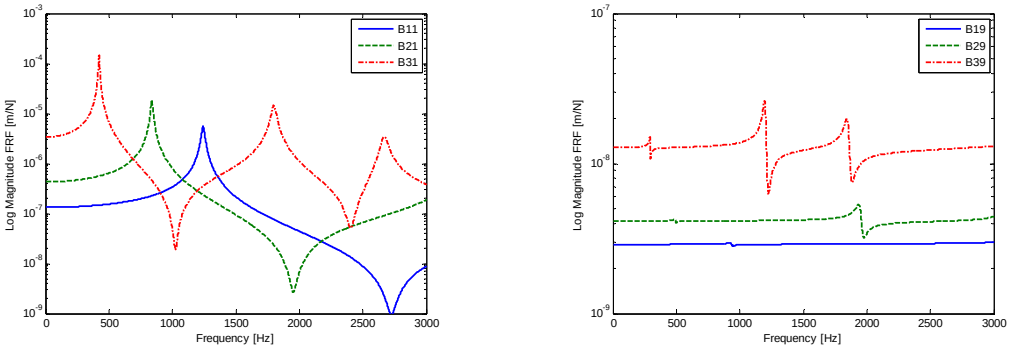

Figure 3.7. FRFs of the workpiece for the steps shown in Figure 3.8

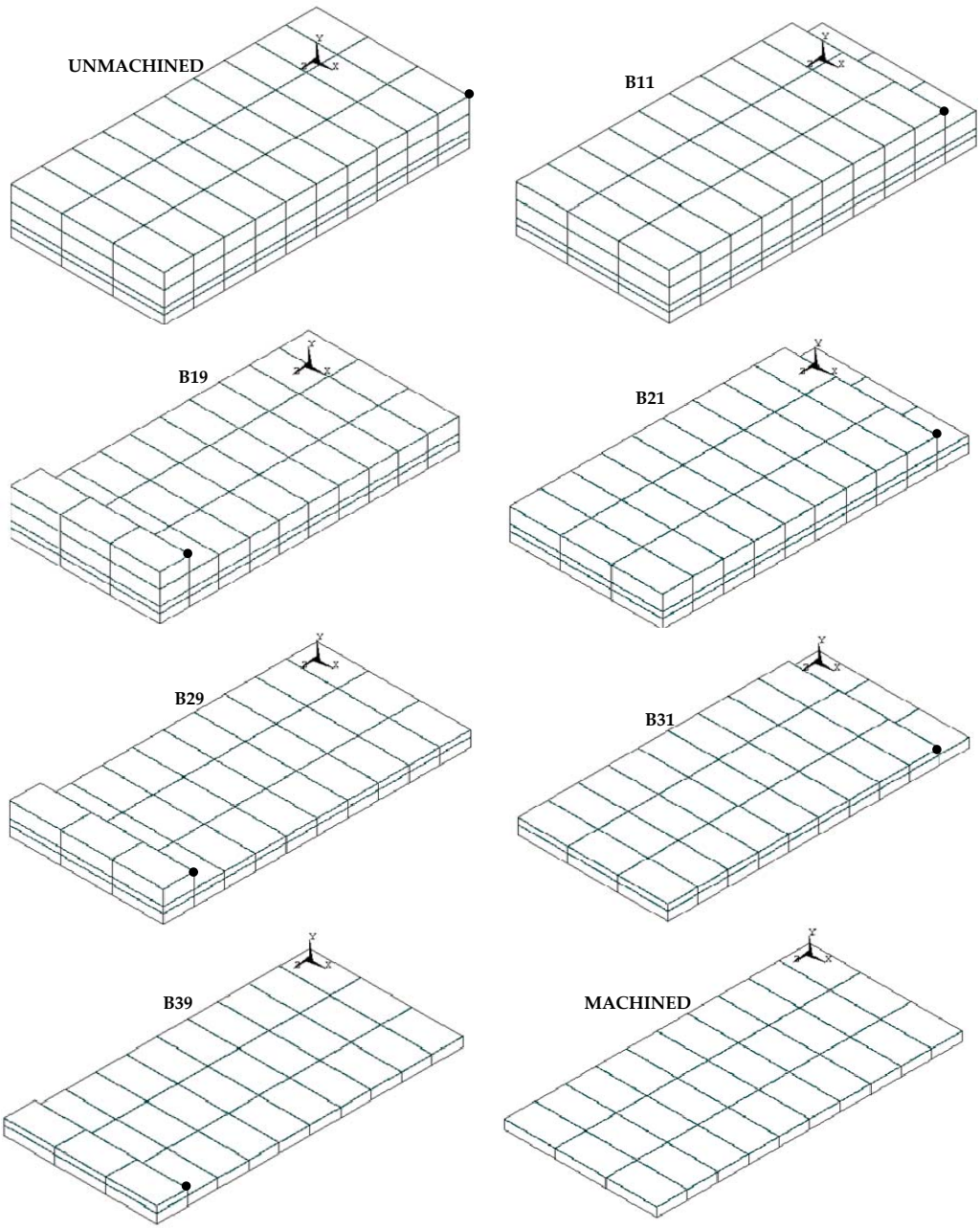

Figure 3.8. 3D mesh models for the steps shown in Figure 3.5

It can be observed that, since the stiffness of the workpiece near to the fixed end is larger than that at other positions, the magnitudes of FRFs are lower near to the fixed end. As also pointed out in [13], as the workpiece is machined, its flexibility increases and comparing with the FRFs of the tool, the dynamics of the workpiece becomes significant in the analysis.

Figure 3.6 and Figure 3.7 show that the results of the developed procedure are in good agreement with the previous study. There are only slight deviations in the magnitudes of the FRFs at the peak points. Also, there are some additional peaks observed in the 3D model. In the present study, the geometry is modeled with more degrees of freedom; hence, the results are more reliable than that of the previous study.

3.4.3 Geometry 3

The third geometry is a blade model, as shown in Figure 3.9.

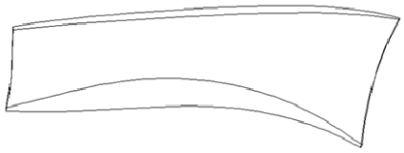

Figure 3.9. Blade analyzed

One of the surfaces of the blade is extruded to obtain a volume to be machined and this extruded volume is divided to five pieces to represent the steps of machining, which can be seen in Figure 3.10.

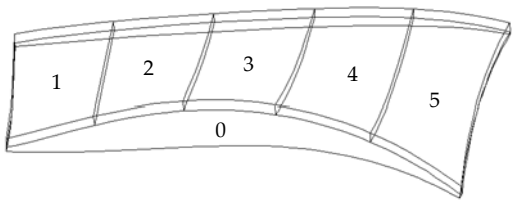

Figure 3.10. Initial volume (0) and volumes machined (1-5) for geometry 2

The mesh generation and modal analysis are performed in Ansys. The meshes for the unmachined and machined workpiece are shown in Figure 3.11.

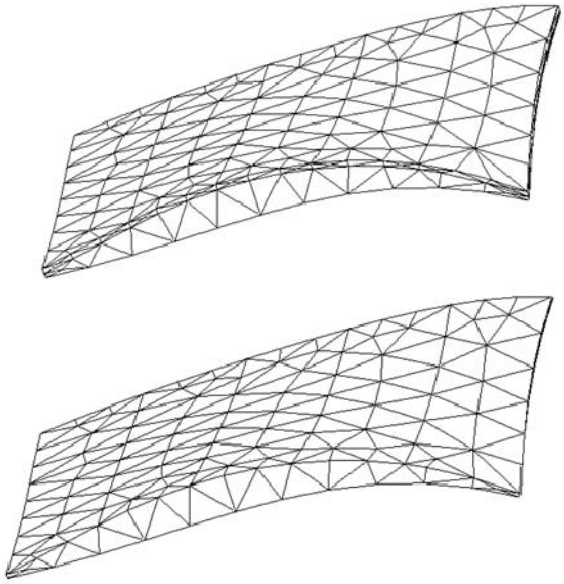

Figure 3.11. Mesh model of unmachined (left) and machined (right) workpiece

Table 3.3 presents the details of the model studied.

Table 3.3. Details about geometry 3

Number of nodes	2208
DOF of initial model	3333
Number of elements added	651

The blade is fixed from one of its surfaces (A1 in Figure 3.9). The machined geometry is analyzed in Ansys. The procedure suggested in this work is followed to obtain the FRFs in different machining stages. These stages and

the nodes whose FRFs are calculated at these stages are shown in Figure 3.12.

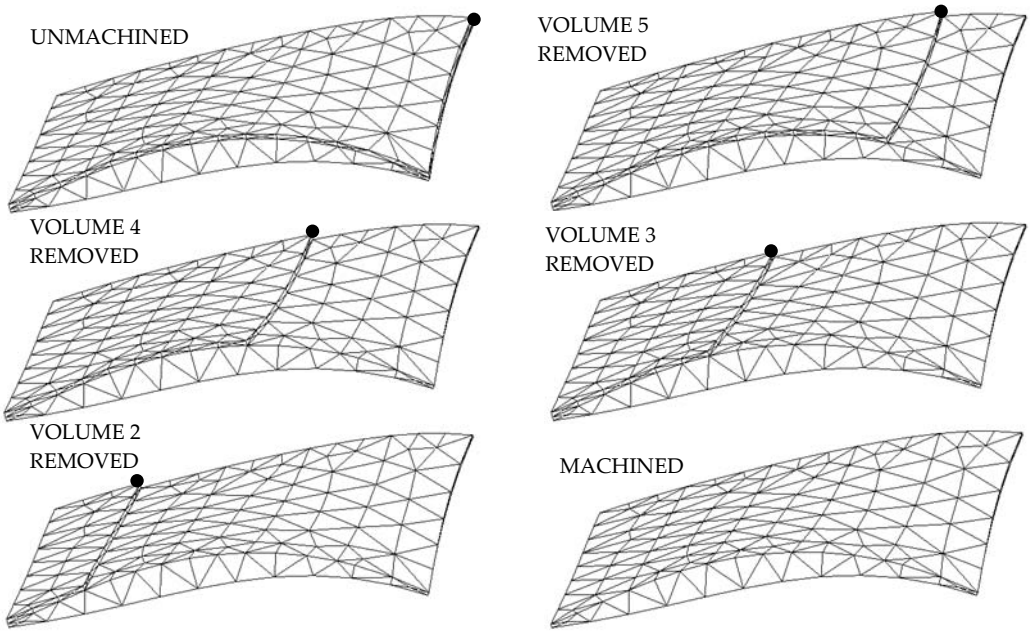

Figure 3.12. Mesh models for the steps of machining the workpiece analyzed

The FRFs predicted for the machining steps shown in Figure 3.12 are plotted in Figure 3.13. Note that in this analysis the initial structure is the machined workpiece, and unmachined geometry is obtained by structural modification. Figure 3.13 shows the first three natural frequencies at the corresponding stages. It can be concluded that as the workpiece is machined, the natural frequencies are shifted and the magnitudes at the peaks of the FRFs also change. In Figure 3.14, the FRF for the unmachined geometry, obtained by the method developed is compared with that obtained by direct modal analysis of the unmachined geometry by using Ansys. The good agreement in two plots reveals the accuracy of the method developed.

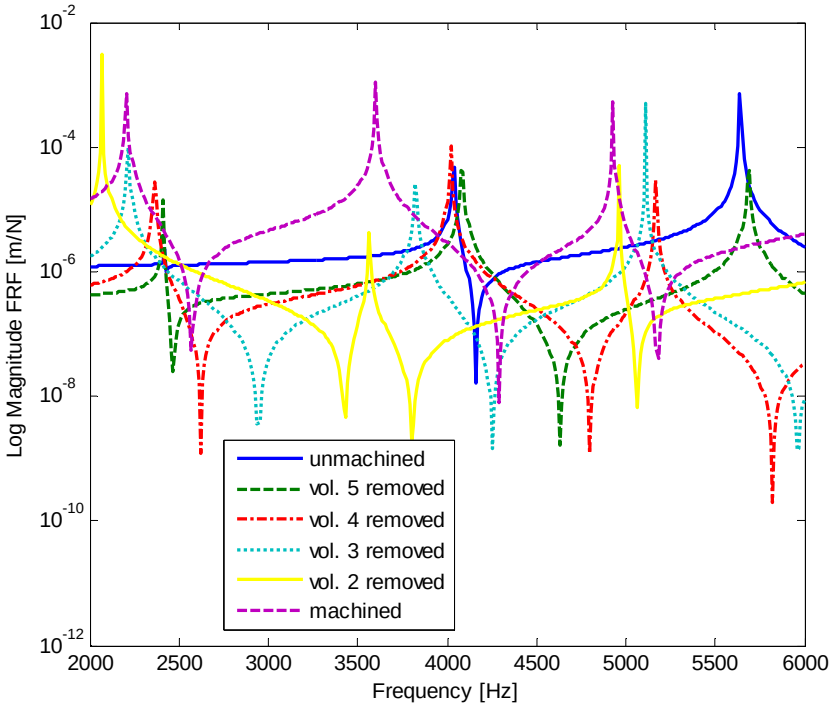

Figure 3.13. Predicted FRFs in the steps shown in Figure 3.12

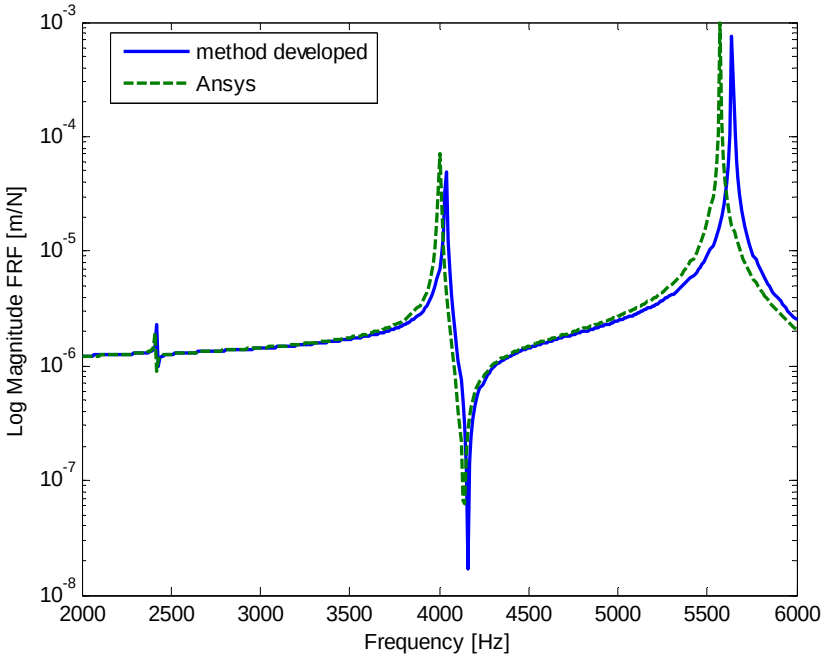

Figure 3.14. FRF of the unmachined workpiece, predicted by the method developed (solid line) and calculated by using Ansys (dashed line)

It should be noted that for the calculation of the FRFs for the initial model, the number of modes used in the computations may be selected to be lower than the total number of modes of the initial model. Using lower number of degrees of freedom will decrease the computation time and the prediction procedure will be faster. However, the predicted FRFs for the machining steps will be less accurate. For the three geometries analyzed in this chapter, all modes of the initial models are used in the computations.

CHAPTER 4

MACHINING STABILITY ANALYSIS FOR DIFFERENT CUTTING STRATEGIES IN THREE AXIS MACHINING

In this chapter, machining of a plate is modeled and stability analysis is performed for different cutting strategies. The dynamics of the plate is predicted for different stages of the machining cycle. Stable cutting conditions are obtained from the machining stability analyses. The effect of workpiece dynamics to productivity is investigated by comparing the results of stability analyses for different strategies.

4.1 Prediction of Workpiece FRF

A plate of dimensions 70 mm (height) × 70 mm (width) × 9.5 mm (thickness) is modeled. The material of the plate is Al 7075 alloy. The plate is to be machined along its thickness, in order to drop the thickness from 9.5 mm to 3 mm. The geometry for the unmachined plate is shown in Figure 4.1.

The material properties are taken as modulus of elasticity of 70 GPa, Poisson's ratio of 0.33 and density of 2800 kg / m^3. Damping of the system is modeled as structural damping with a damping coefficient of 1.52%.

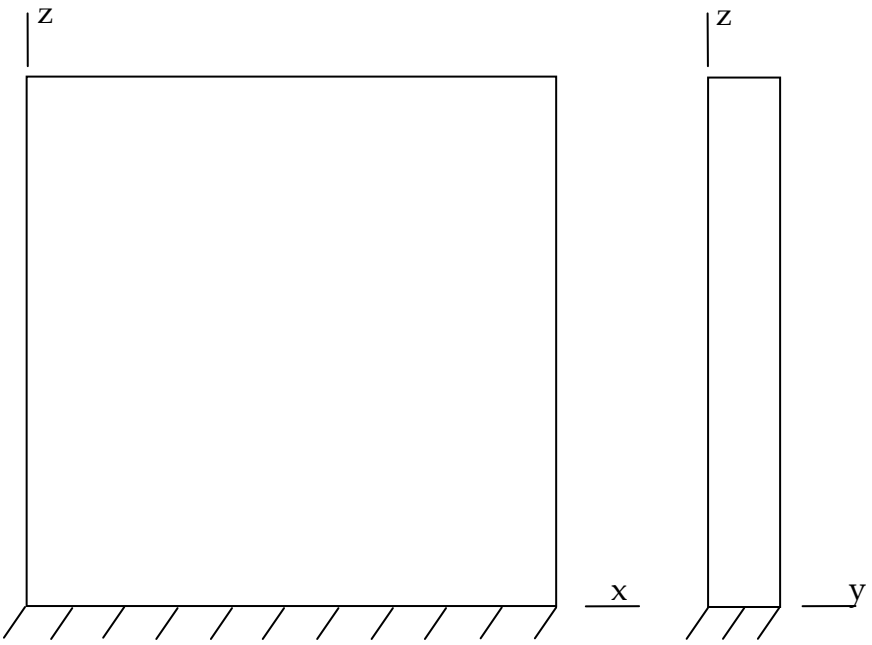

Figure 4.1. Geometry for the unmachined plate

The machining of the plate is modeled as the removal of the volume parts, in three steps in x and y directions, and in five steps in z direction. Different cases will be analyzed for different thickness change during machining. The thickness of the layer removed is the radial depth of cut of the machining step. In machining stability analysis, smaller radial depth of cut results in larger stability limits for the axial depth of cut. The thicknesses of the layers removed are modeled to decrease in order, so that for the semi-finishing and finishing cuts more stable cutting conditions are obtained.

A total of six strategies will be analyzed. Three of the strategies modeled are layer removal strategies and the other three are step removal strategies. In layer removal, the thickness is reduced for all the layer of the plate, whereas in step removal, the thickness is reduced to its final value for each step. Figure 4.2 and Figure 4.3 show the machining stages of layer and step removals, respectively.

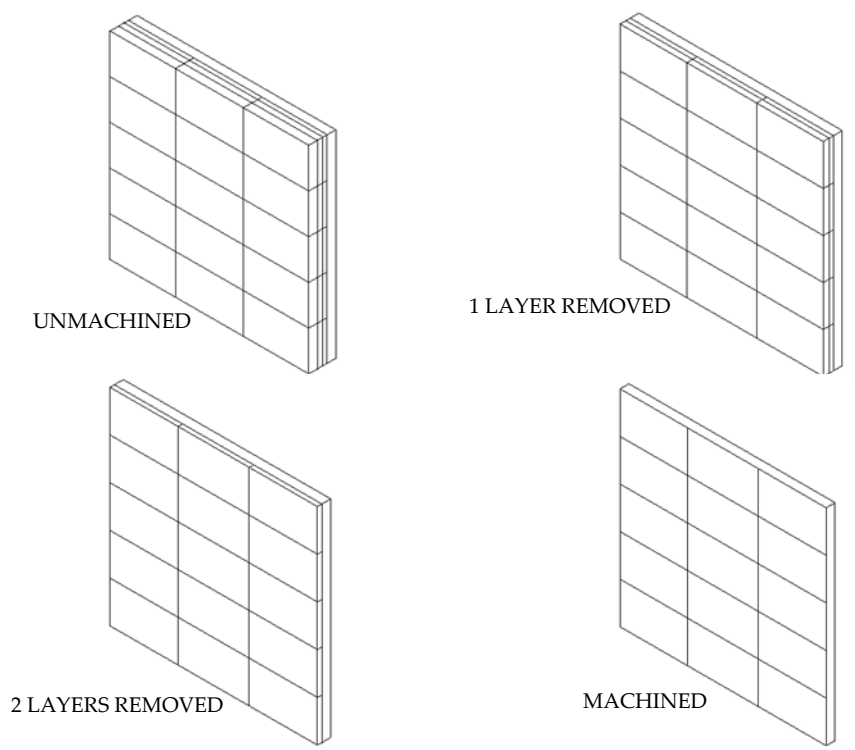

Figure 4.2. Stages of a layer removal process

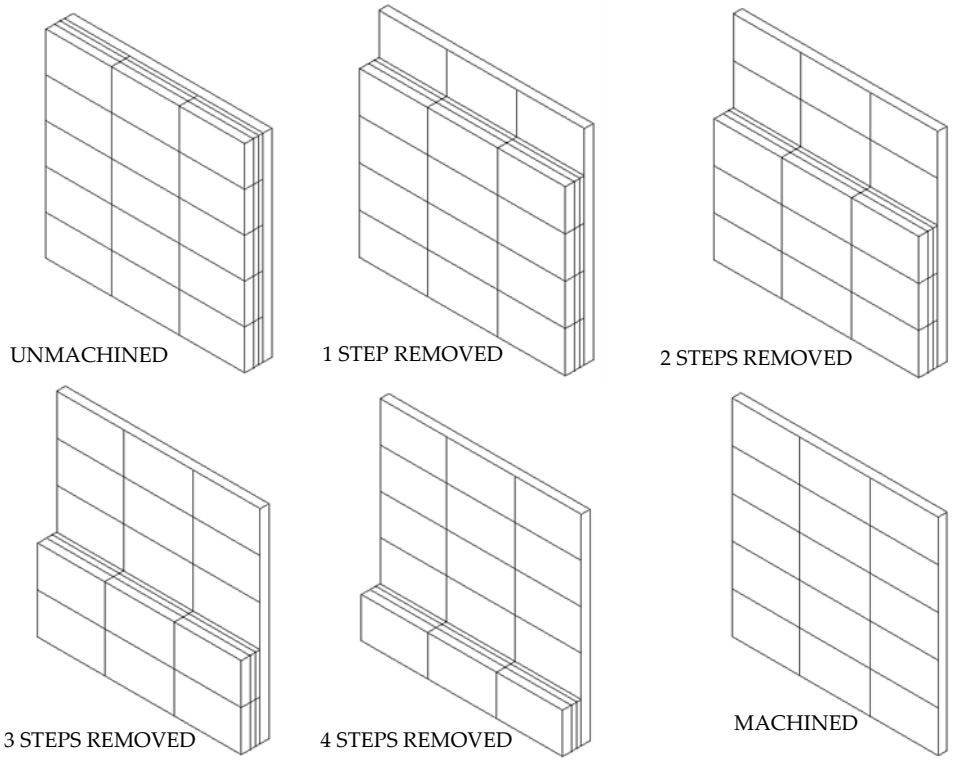

Figure 4.3. Stages of a step removal process

The removal type and the thicknesses of the layers for the strategies modeled are given in Table 4.1.

Table 4.1. Removal types and layer thicknesses of the strategies

Strategy	Removal type	Thickness of the 1st layer (mm)	Thickness of the 2nd layer (mm)	Thickness of the 3rd layer (mm)	Thickness of the final layer (mm)
A	layer	3.0	2.0	1.5	3.0
B	layer	4.0	1.5	1.0	3.0
C	layer	5.0	1.0	0.5	3.0
D	step	3.0	2.0	1.5	3.0
E	step	4.0	1.5	1.0	3.0
F	step	5.0	1.0	0.5	3.0

Thickness change for case A: 9.5 mm – 6.5 mm – 4.5 mm – 3 mm. The volume division for case A is shown in Figure 4.4.

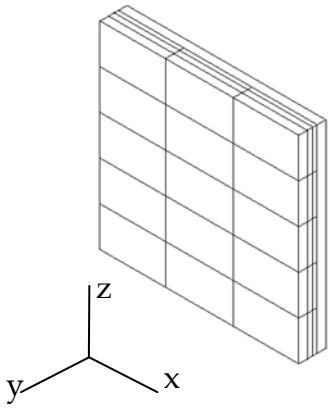

Figure 4.4. Volume division for strategy A

To indicate the position of machining, a coding convention is used as A_1_1_1. Here, the letter denotes the cutting strategy applied and the numbers stand for the corresponding cutting steps in y, z and x directions. The step A_1_1_1 is the removal of the first element from the unmachined workpiece.

Using the procedure described in Chapter 3, the dynamics of the workpiece at each step is predicted. The FRFs, in x and y directions, of the workpiece for the step A_1_1_1, i.e. the unmachined stage, are plotted in Figure 4.5 and Figure 4.6. The first two natural frequencies of the unmachined plate are 1616 and 3679 Hz, respectively, so the FRFs are plotted in a frequency range of 0-4000 Hz. Note that, these are the receptances for the point that is in contact with the tool.

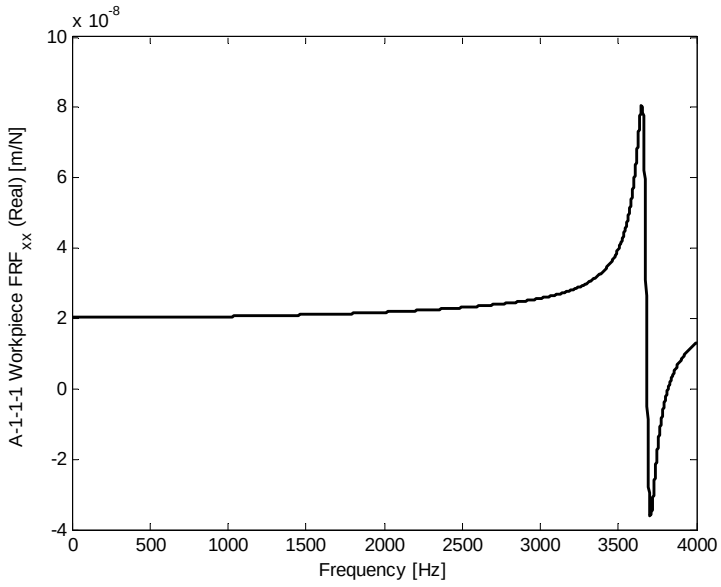

Figure 4.5. Workpiece FRF_{xx} for the step A_1_1_1 (unmachined stage)

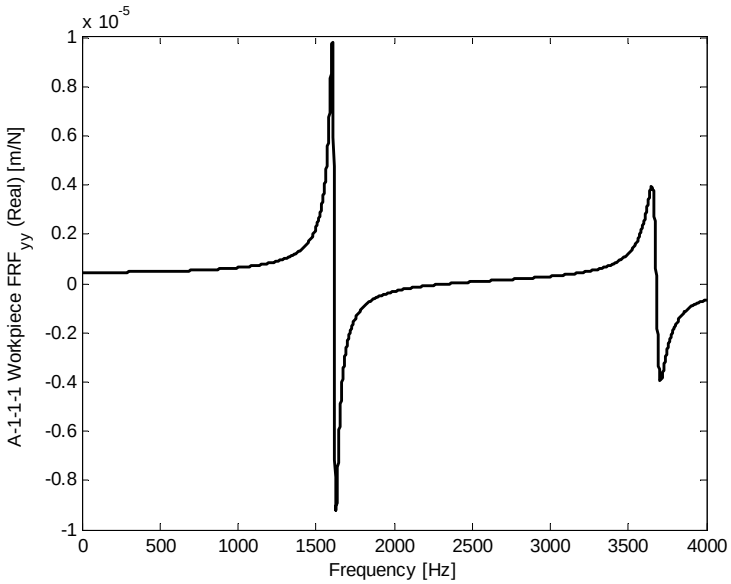

Figure 4.6. Workpiece FRF_{yy} for the step A_1_1_1 (unmachined stage)

For the successive machining steps in x direction, steps A_1_1_1, A_1_1_2 and A_1_1_3 as shown in Figure 4.7, the change in the FRF, in x and y directions respectively, of the workpiece is shown in Figure 4.8 and Figure 4.9.

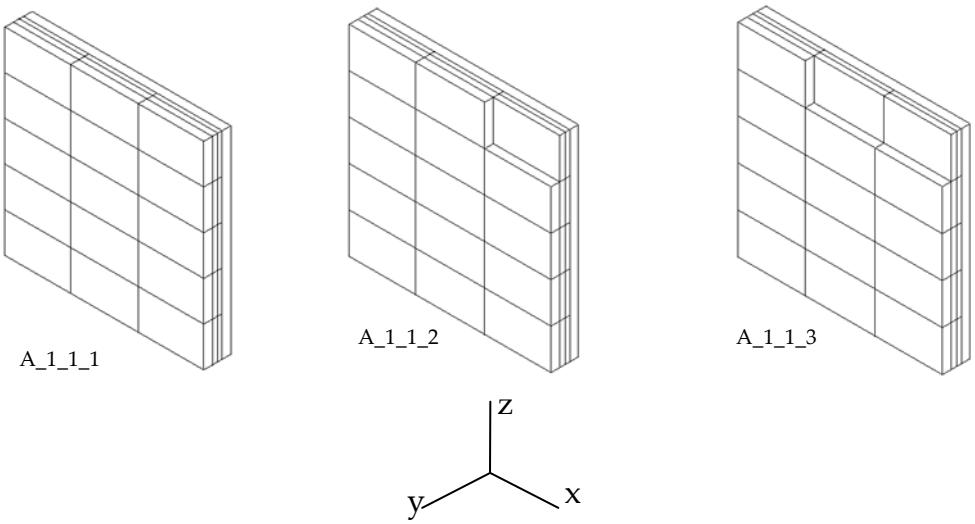

Figure 4.7. Successive machining steps in x direction

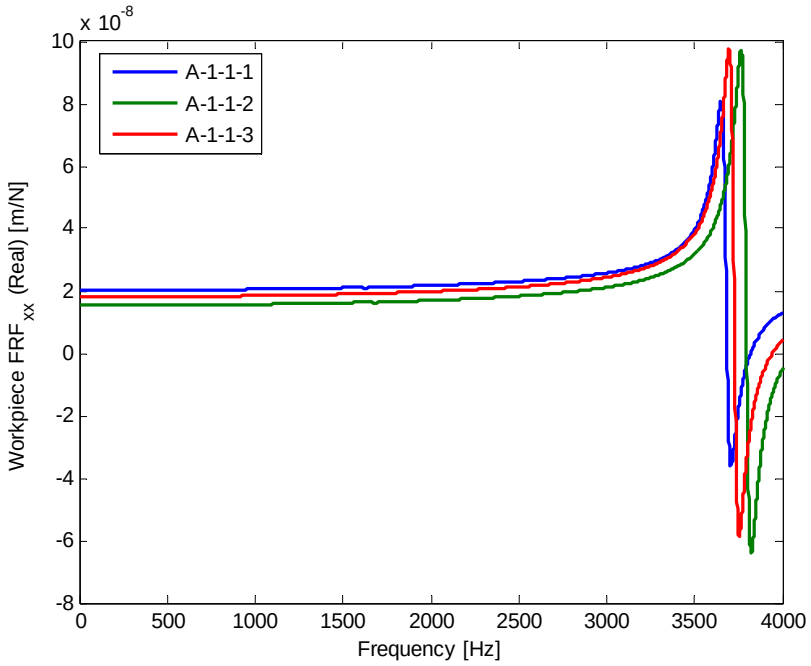

Figure 4.8. Workpiece FRF_{xx} for the steps A_1_1_1, A_1_1_2 and A_1_1_3

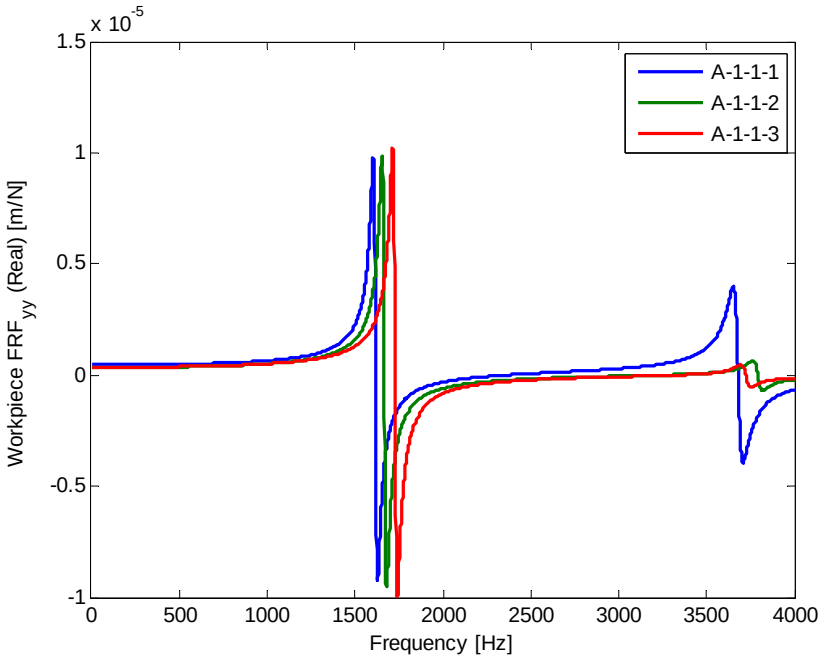

Figure 4.9. Workpiece FRF_{yy} for the steps A_1_1_1, A_1_1_2 and A_1_1_3

For different steps in z direction, steps A_1_1_1, A_1_2_1, A_1_3_1, A_1_4_1, and A_1_5_1 as shown in Figure, the change in the FRFs, in x and y directions respectively, of the workpiece can be seen in Figure 4.11 and Figure 4.12. The magnitude of the receptance around the fixed end of the workpiece has lower value than that near to the free end. The stiffness of the workpiece is higher at the fixed end side, as expected.

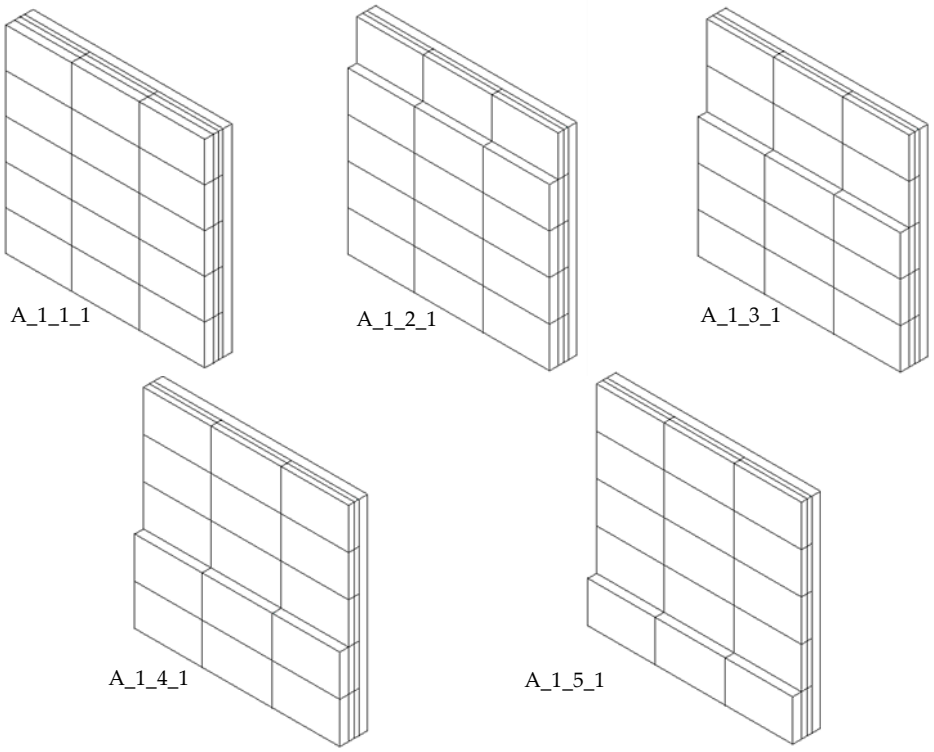

Figure 4.10. Different steps in z direction

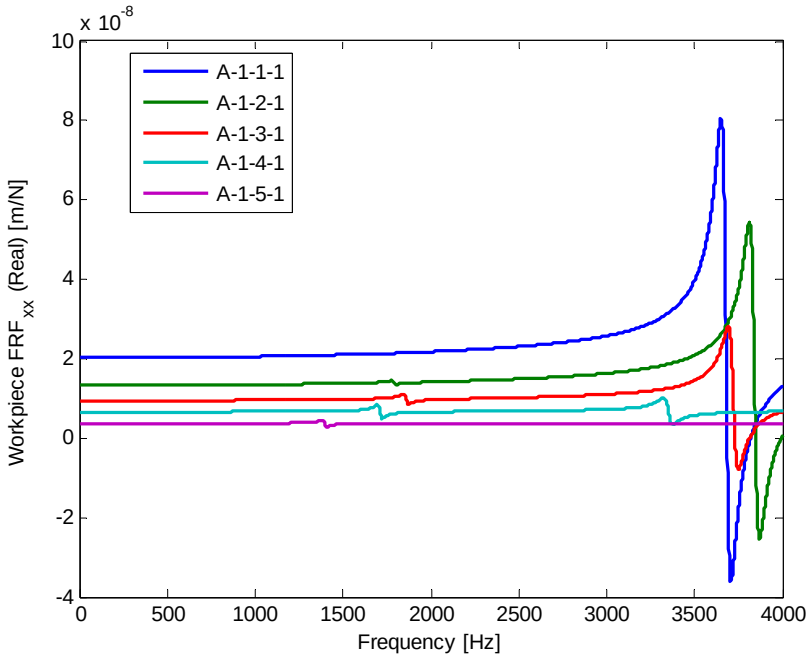

Figure 4.11. Workpiece FRF_{xx} for the steps A_1_1_1, A_1_2_1, A_1_3_1, A_1_4_1 and A_1_5_1

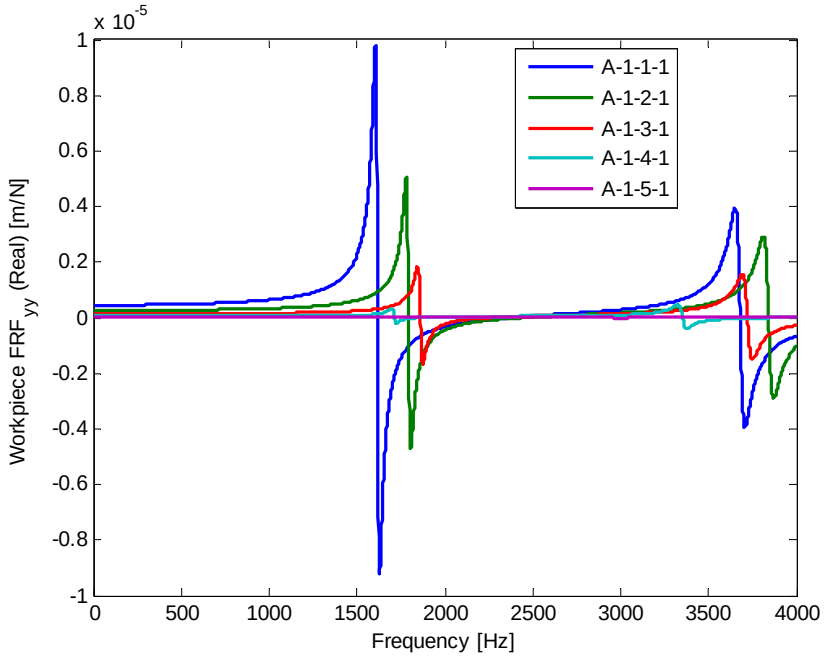

Figure 4.12. Workpiece FRF_{xx} for the steps A_1_1_1, A_1_2_1, A_1_3_1, A_1_4_1 and A_1_5_1

The effect of the decreased thickness on the part dynamics can be seen plotting the FRFs at the first steps of each layer which are shown in Figure 4.13. The FRFs at these steps are shown in Figure 4.14 and Figure 4.15. The workpiece becomes more flexible as its thickness is reduced and the magnitudes of the FRFs increase.

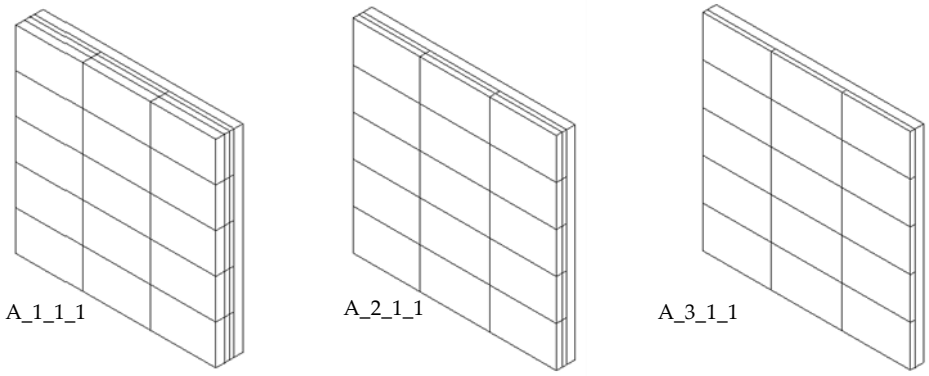

Figure 4.13. Different steps in y direction

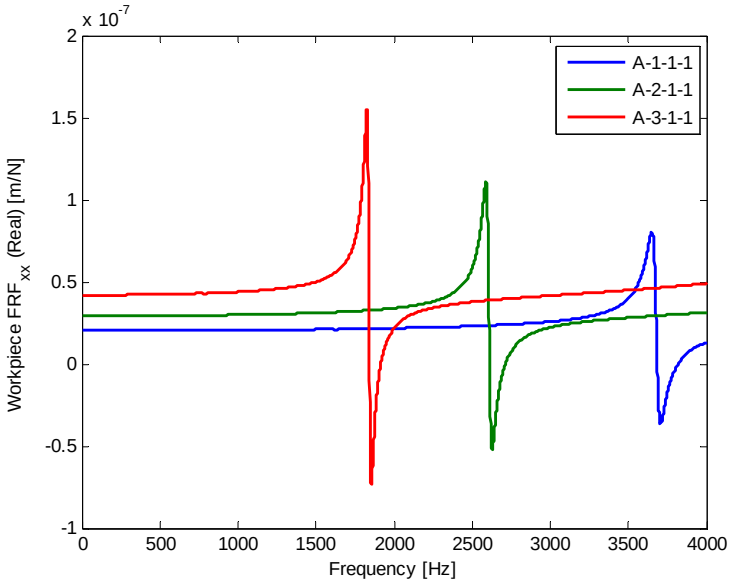

Figure 4.14. Workpiece FRF_{xx} for the steps A_1_1_1, A_2_1_1 and A_3_1_1

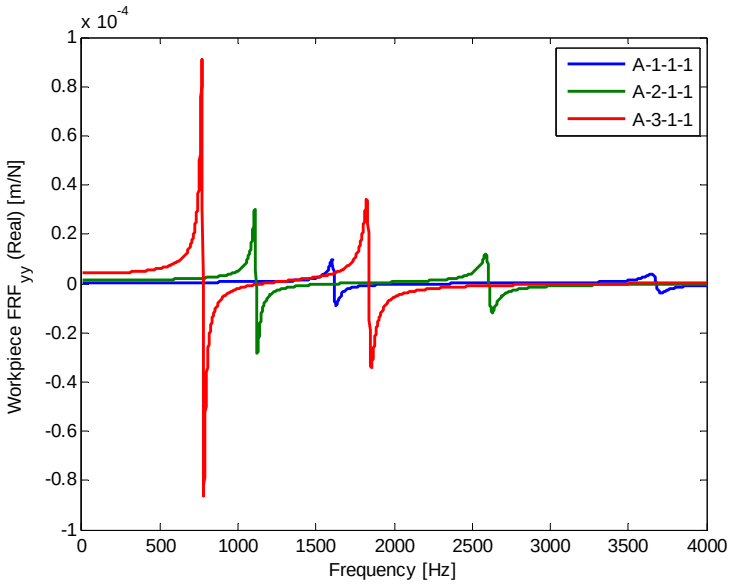

Figure 4.15. Workpiece FRF_{xx} for the steps A_1_1_1, A_2_1_1 and A_3_1_1

4.2 Effects of Workpiece Flexibility to Stability Diagrams

The FRFs of the workpiece at all the steps are used in the machining stability analysis to determine the chatter free depth of cuts. The stability analysis is handled by using the software Cutpro, a machining simulation program developed by the Manufacturing Automation Laboratories of University of British Columbia. Note that, the experimentally obtained tool point FRFs are used in the analysis to include the dynamics of the spindle-holder-tool system. The FRFs, in x and y directions, of the tool used in the analysis are given in Figure 4.16 and Figure 4.17.

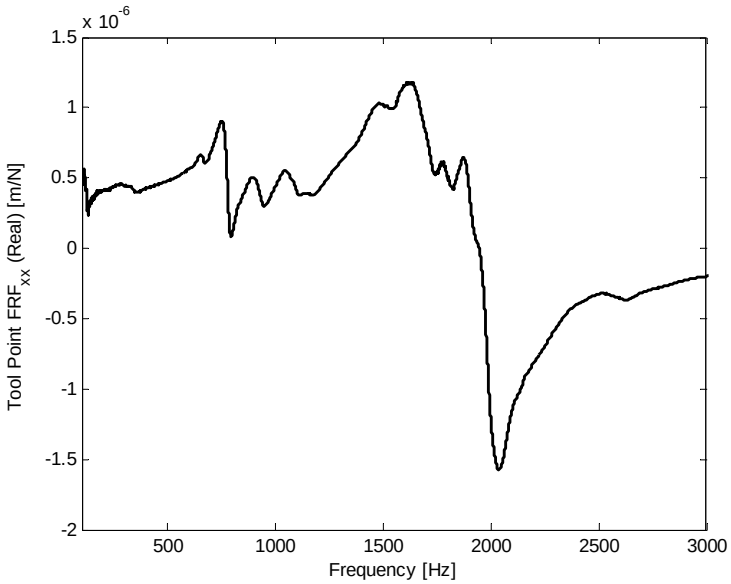

Figure 4.16. Tool point FRF_{xx}

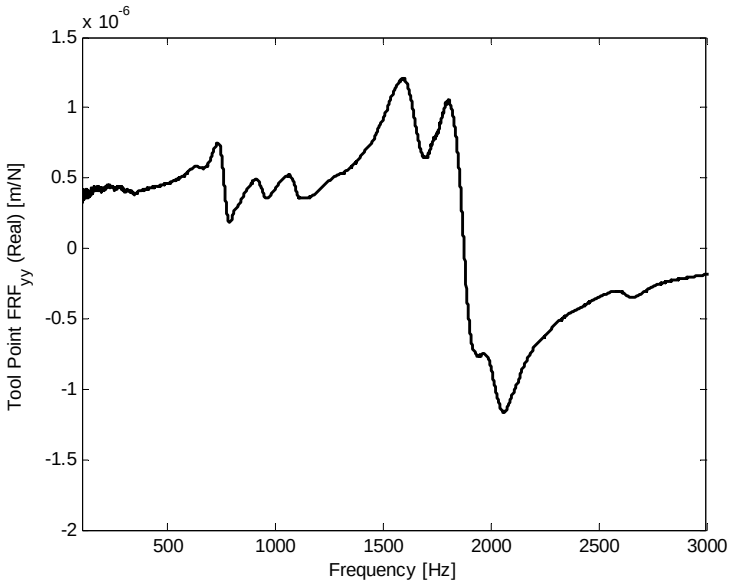

Figure 4.17. Tool point FRF_{yy}

For the known dynamics of the tool and the workpiece, the machining analysis is carried out. The tool used is a cylindrical end, uniform four-fluted tool. The material of the tool is carbide, the diameter is 6 mm, the helix angle is 30° and the relief and rake angles are 5° each. Average cutting

coefficient is assumed in the analysis. The spindle direction is clockwise and the milling mode is down-milling with a feed rate of 0.1 mm/flute. The radial depth of cut is the thickness change of the workpiece and it has the values of 3 mm, 2 mm and 1.5 mm in corresponding layers in strategy A. Figure 4.18 shows the axial and radial depths of cut for the machining of the aluminum plate.

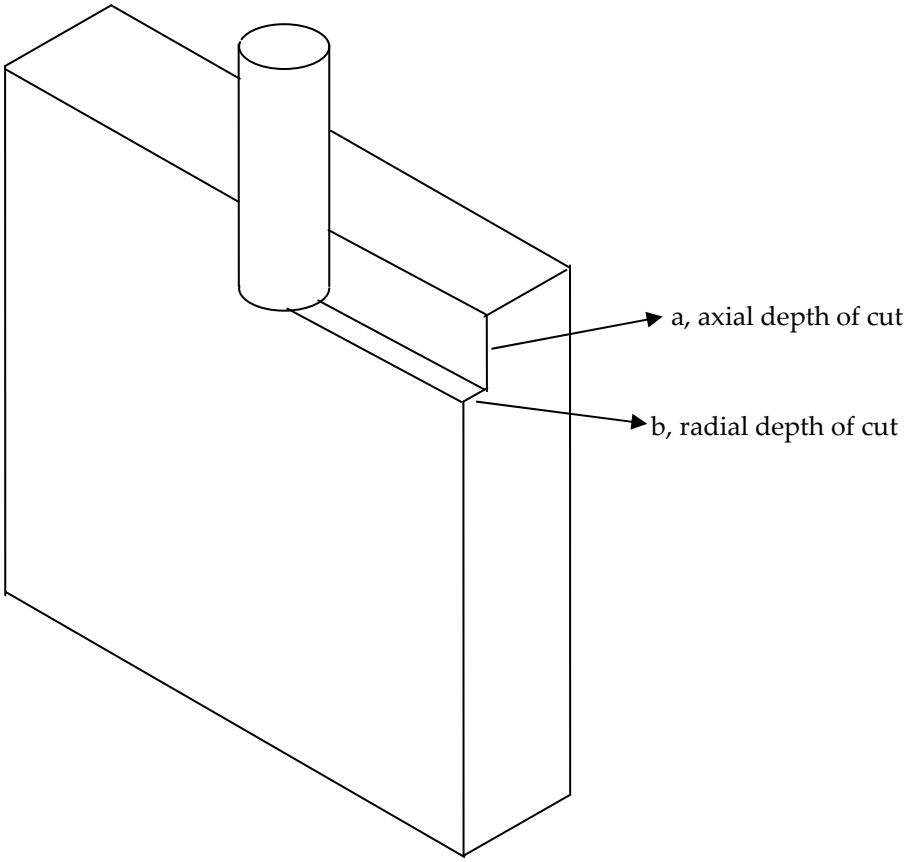

Figure 4.18. Axial and radial depths of cut for the machining process

The stability lobe diagrams obtained using Cutpro for the steps A_1_1_1, A_1_1_2 and A_1_1_3 are shown in Figure 4.19. The dynamics of the workpiece does not change significantly between these steps, so the stability lobes have quite similar limits. The shifts in the lobes show that it

would be practical to use the absolute limiting depth of cuts for the passes along the width direction.

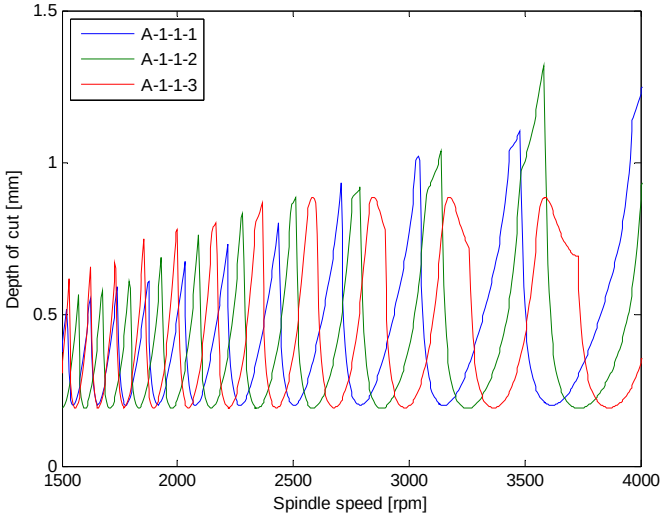

Figure 4.19. Stability limits for the steps A_1_1_1, A_1_1_2 and A_1_1_3

The stability lobe diagrams for the steps A_1_1_1, A_1_2_1, A_1_3_1, A_1_4_1 and A_1_5_1 are plotted in Figure 4.20. As the stiffness of the workpiece increases, the limiting depth of cut increases.

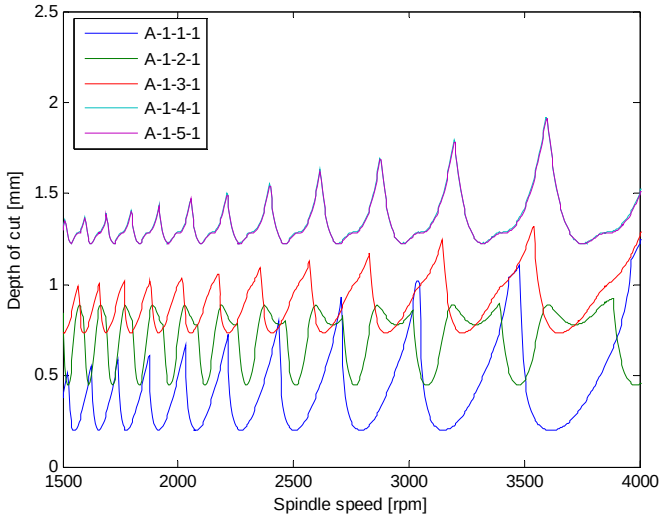

Figure 4.20. Stability limits for the steps A_1_1_1, A_1_2_1, A_1_3_1, A_1_4_1, and A_1_5_1

The stability diagrams for the initial steps of each layer removal are shown in Figure 4.21. The flexibility increases as the thickness is reduced, and the stable depth of cut decreases.

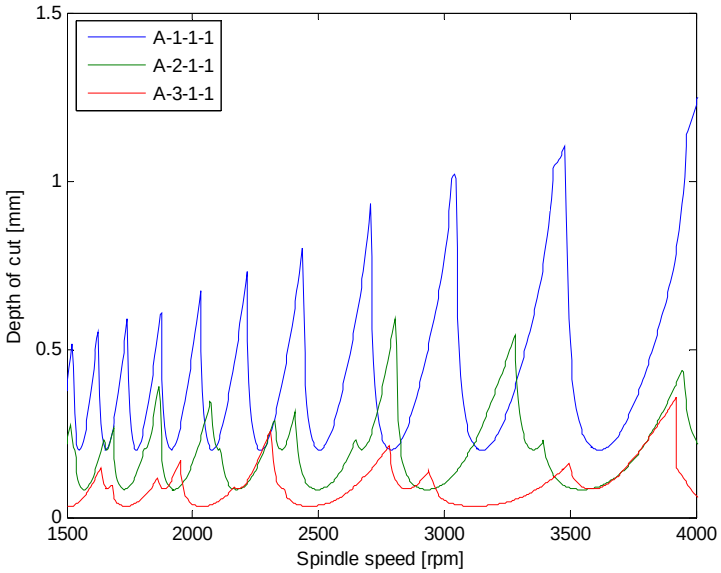

Figure 4.21. Stability limits for the steps A_1_1_1, A_2_1_1 and A_3_1_1

4.3 Different Cutting Strategies

The machining of the plate is modeled with six different cutting strategies. In this section, these strategies are described in detail. The limiting stable depths of cut for each step of the strategies are given. The manufacturing times for the strategies are compared.

4.3.1 Stable Depths of Cut for Different Cutting Strategies

The stability limits obtained by Cutpro for the strategy A is given in Table 4.2. The stability limits for the same radial depth of cut increase, near to the fixed end of the plate.

Table 4.2. Stability limits for the steps for strategy A

Step	A1_ (9.5 mm – 6.5 mm)	A2_ (6.5 mm – 4.5 mm)	A3_ (4.5 mm – 3.0 mm)
_1_1	0.20	0.08	0.03
_1_2	0.19	0.08	0.03
_1_3	0.19	0.08	0.03
_2_1	0.45	0.16	0.07
_2_2	0.39	0.15	0.06
_2_3	0.34	0.14	0.06
_3_1	0.73	0.46	0.19
_3_2	0.89	0.38	0.15
_3_3	1.01	0.37	0.15
_4_1	1.22	1.86	0.85
_4_2	1.20	1.73	0.72
_4_3	1.21	1.78	0.71
_5_1	1.22	1.80	2.44
_5_2	1.22	1.78	2.36
_5_3	1.22	1.78	2.36

The minimum of the three stability limits along x direction should be taken as the limiting depth of cut in the corresponding step. Table 4.2 can be simplified to Table 4.3.

Table 4.3. Stability limits for strategy A (simplified for variation along width direction)

Step	A1_ (9.5 mm – 6.5 mm)	A2_ (6.5 mm – 4.5 mm)	A3_ (4.5 mm – 3.0 mm)
_1	0.19	0.08	0.03
_2	0.34	0.14	0.06
_3	0.73	0.37	0.15
_4	1.20	1.73	0.71
_5	1.22	1.78	2.36

Table 4.4, Table 4.5, Table 4.6, Table 4.7 and Table 4.8 present the limiting depths of cut for strategies B to F.

Table 4.4. Stability limits for strategy B

Step	B1_ (9.5 mm – 5.5 mm)	B2_ (5.5 mm – 4.0 mm)	B3_ (4.0 mm – 3.0 mm)
_1	0.17	0.06	0.03
_2	0.26	0.11	0.05
_3	0.48	0.27	0.14
_4	0.94	1.26	0.62
_5	0.94	2.27	3.48

Table 4.5. Stability limits for strategy C

Step	C1_ (9.5 mm – 4.5 mm)	A2_ (4.5 mm – 3.5 mm)	A3_ (3.5 mm – 3.0 mm)
_1	0.15	0.04	0.03
_2	0.27	0.08	0.06
_3	0.45	0.20	0.15
_4	0.78	0.81	0.64
_5	0.78	3.42	6.61

Table 4.6. Stability limits for strategy D

Step	D1_ (9.5 mm – 6.5 mm)	D2_ (6.5 mm – 4.5 mm)	D3_ (4.5 mm – 3.0 mm)
_1	0.19	0.22	0.28
_2	0.36	0.42	0.43
_3	1.43	0.89	1.20
_4	1.23	1.81	1.60
_5	1.22	1.78	2.36

Table 4.7. Stability limits for strategy E

Step	E1_ (9.5 mm – 5.5 mm)	E2_ (5.5 mm – 4.0 mm)	E3_ (4.0 mm – 3.0 mm)
_1	0.17	0.27	0.36
_2	0.31	0.48	0.52
_3	0.67	1.39	1.35
_4	0.95	2.19	3.03
_5	0.94	2.33	3.48

Table 4.8. Stability limits for strategy F

Step	F1_ (9.5 mm – 4.5 mm)	F2_ (4.5 mm – 3.5 mm)	F3_ (3.5 mm – 3.0 mm)
_1	0.15	0.37	0.58
_2	0.29	0.58	0.78
_3	0.56	1.55	1.64
_4	0.78	2.26	3.71
_5	0.78	3.45	6.61

4.3.2 Machining Times for Different Cutting Strategies

The height for each step modeled is 14 mm. Number of passes required to remove material of height 14 mm can be calculated by rounding to the first integer greater than the ratio of the height to the limiting depth of cut.

$$nop = roundup\left(\frac{h}{a_{\lim}}\right) \tag{4.1}$$

Number of passes required for the strategy A can be calculated using the limiting depths of cut values listed in Table 4.3. Table 4.9 shows the number of passes for each step for strategy A.

Table 4.9. Number of passes for the steps of strategy A

Step	A1_	A2_	A3_
_1	74	175	467
_2	42	100	234
_3	20	38	94
_4	12	9	20
_5	12	8	6
		Total	1311

Table 4.10 gives the total number of passes for strategies A to F.

Table 4.10. Total number of passes for six strategies

Strategy	Total number of passes
A	1311
B	1505
C	1652
D	387
E	374
F	348

The machining time for one pass is related with the width (w) of the workpiece removed in the pass and the feed rate (V_f). The width is 70 mm and the same for all passes. The feed rate depends on the feed rate per flute (f), the number of flutes on the cutter (N) and the spindle speed (n). The feed rate per flute is taken as 0.1 mm/flute. The number of flutes on the cutter is four and the spindle speed is taken 3000 rpm in the analyses. The feed rate in mm/s can be calculated as:

$$V_f = \frac{N \cdot f \cdot n}{60} = \frac{4 \cdot 0.1 \cdot 3000}{60} = 20\ mm/s \tag{4.2}$$

The machining time for one pass can now be obtained as:

$$t = \frac{w}{V_f} = \frac{70\ mm}{20\ mm/s} = 3.5\ s \tag{4.3}$$

The machining times for the six strategies are listed in Table 4.11.

Table 4.11. Manufacturing time for six strategies

Strategy	Machining time (s)
A	4588.5
B	5267.5
C	5782
D	1354.5
E	1309
F	1218

It can be concluded that step removal is superior to the layer removal in terms of productivity. For the same thickness variations, step removal strategies require much less time than the layer removal strategies. For layer removal, the productivity decreases if the thickness removed in the rough cut is increased and the thickness removed in the semi-finishing and finishing cuts are decreased. In the step removal strategies, increasing the thickness removed in the rough cut and decreasing those in the semi-finishing and finishing cuts, the productivity increases.

CHAPTER 5

MACHINING STABILITY ANALYSIS FOR FIVE AXIS MACHINING

In this chapter, the procedure developed is applied to a five axis machining process of a blade. For the predicted part dynamics of the blade throughout the machining cycle, machining stability analyses are performed. Different production strategies are compared for the productivity in the finishing cuts.

5.1 Production Strategies

The geometry of the machined blade is shown in Figure 5.1. Blade is machined on a hub as seen in Figure 5.2. The production of the blade on the hub can be divided into three cycles: rough cut, semi-finishing cut and finishing cut. In the rough cut, the disc is machined to obtain the slots for the blade. After the semi-finishing and finishing cuts, the final accurate surfaces of the blade are produced. It can be assumed that the workpiece dynamics in the rough cut does not affect the system dynamics, and thus neither the stability of the machining. As the blade gets much thinner in semi-finishing and finishing cuts, its dynamics becomes significant for stability.

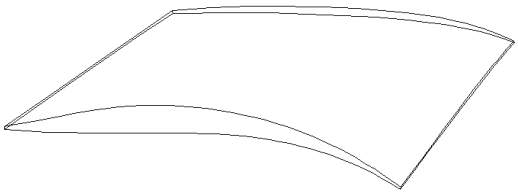

Figure 5.1. Geometry of the blade analyzed

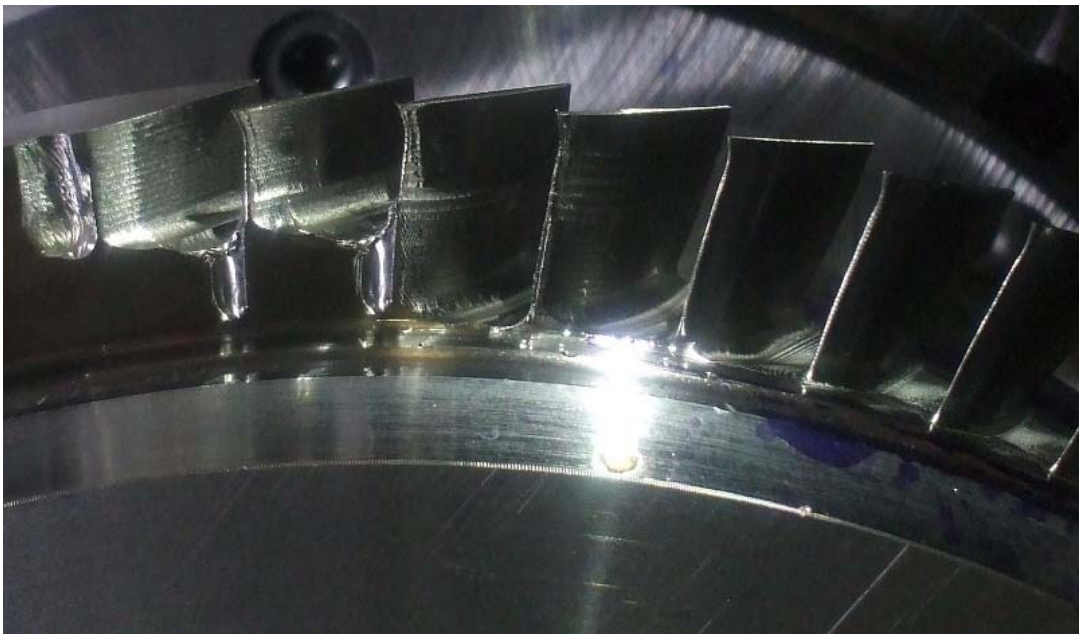

Figure 5.2. A typical hub and blades machined on the hub

The three cycles can be schematically shown in profile view of the blade as in Figure 5.3.

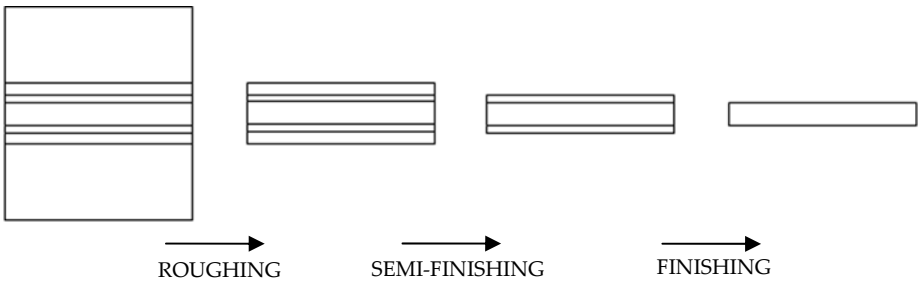

Figure 5.3. Three machining cycles in profile view

The number of the steps of the material removal in the rough cut is different for different production strategies which will be compared in the following sections. In one approach, the material in the roughing cycle can be removed in a single step, and then the semi-finishing and finishing cycles can be performed. Figure 5.4 shows the steps of a single roughing machining.

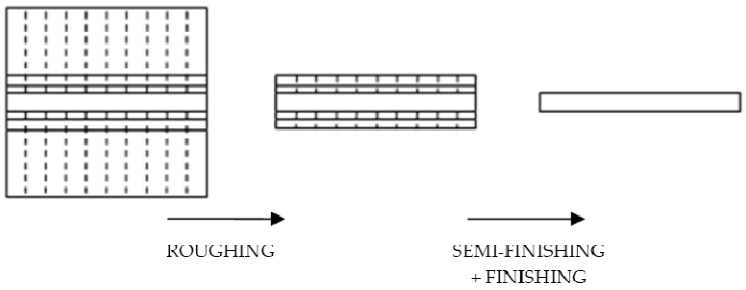

Figure 5.4. Steps of a single roughing machine (Strategy A)

It is also possible to divide the roughing into two or more steps and perform the semi-finishing and finishing cuts after each of these steps. The length of the machined part of the blade outside the hub will be smaller with more number of steps in roughing cut, and this will result in much stiffer blade and much stable finishing. The number of steps in the roughing strategies A, B and C is one, two and three, respectively. The single roughing cycle shown in Figure 5.4 is performed in strategy A. As seen in Figure 5.5, in strategy B, roughing is performed in two cycles: in the first cycle, half of the material is removed and in the second cycle, for the remaining half is removed.

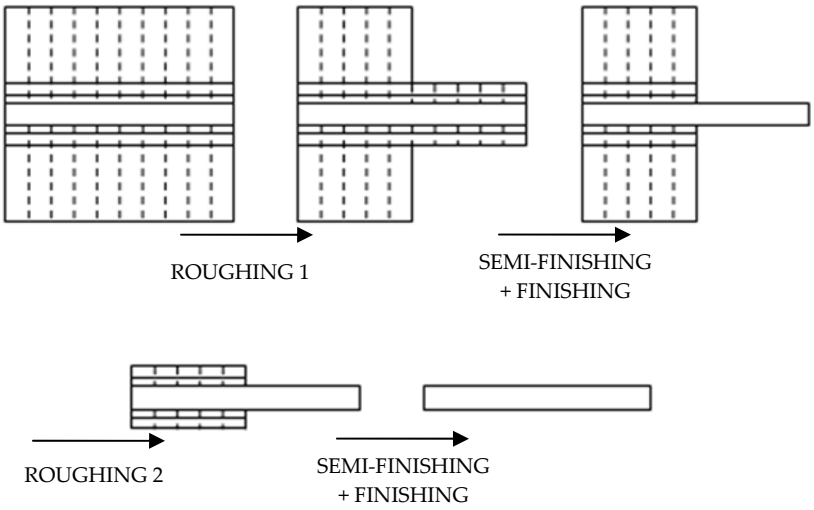

Figure 5.5. Steps of machining with two stages in roughing (Strategy B)

In strategy C, in the first step of the rough cut, 30% of the material is removed. In the second cut, 30% more material is removed and finally in the third step, the roughing is completed. Figure 5.6 shows the steps of machining in strategy C.

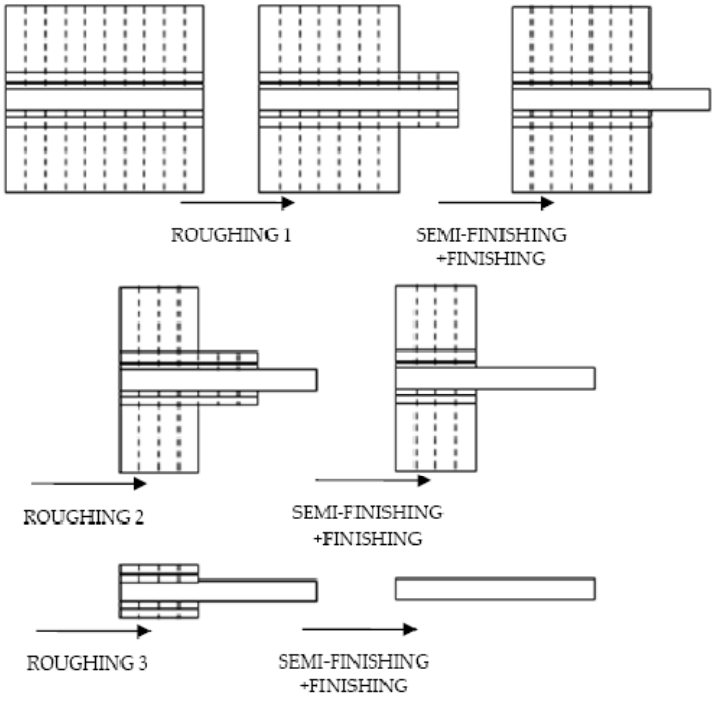

Figure 5.6. Steps of machining with three stages in roughing (Strategy C)

If it is assumed that the part dynamics does not affect the stability in roughing cycles, the production times for roughing cycles for the strategies will be the same. To analyze the effect of the part dynamics to productivity of the process, the stability limits in the semi-finishing and finishing cuts are required to obtain the production times at these cuts. To simplify the analysis, finishing of only one of the surfaces will be analyzed. Being dependent on the change in the part dynamics, the productivity for finishing the other surface and the semi-finishing of both surfaces may be expected to have a similar behavior to the case analyzed.

The finishing of one of the surfaces of the blade will be analyzed for the three strategies. The thickness of the material removed in the finishing step is 0.5 mm. The finishing cut is modeled as a ten step procedure. The blade can be modeled as it is clamped from the surface connected to the hub. For strategies B and C, the finishing at the intermediate stages can also be modeled as clamped from the surface roughed.

The steps of strategies A, B and C are shown in Figure 5.7, Figure 5.8 and Figure 5.9, in side view, respectively.

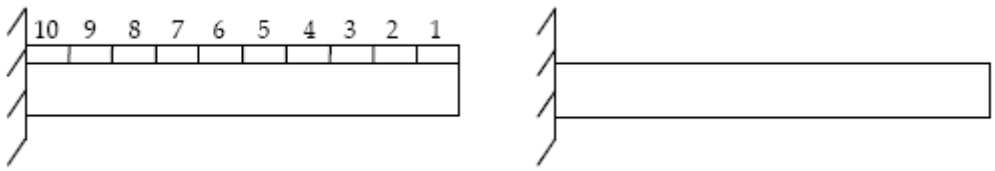

Figure 5.7. Finishing steps in strategy A

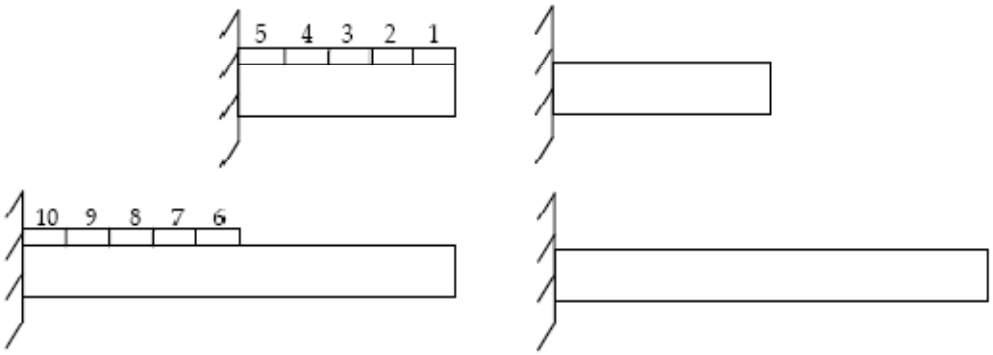

Figure 5.8. Finishing steps in strategy B

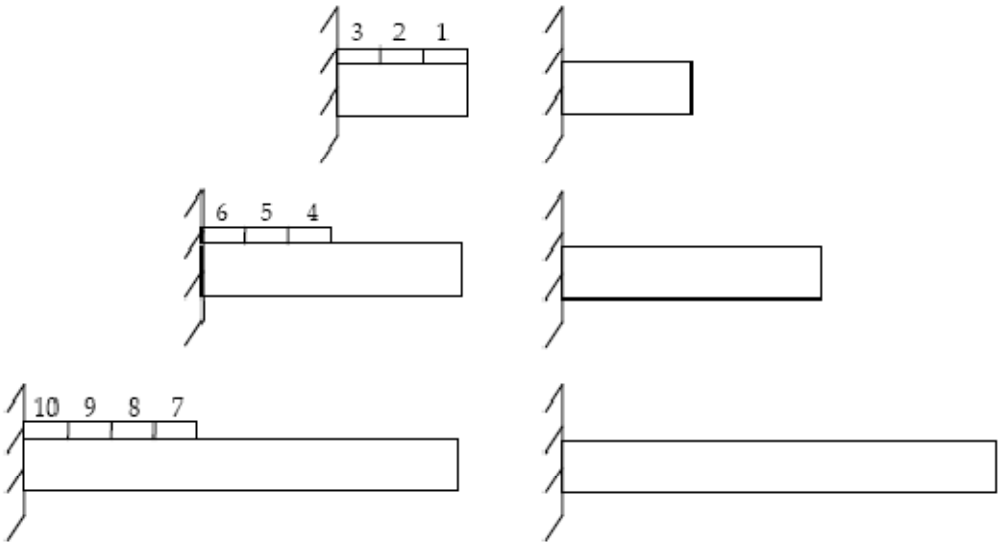

Figure 5.9. Finishing steps in strategy C

5.2 Details of the Machining Process

The type of the tool is ball end and it is uniform four-fluted. Tool material is carbide, tool diameter is 8 mm and helix, relief and rake angles are 30°, 5° and 5°, respectively. Average cutting coefficient is assumed. Spindle

direction is counter-clockwise and the feed rate is 0.12 mm/flute. The radial depth of cut is 0.5 mm, which is the same for the three strategies.

The material of the blade is titanium alloy Ti-6Al-4V. The modulus of elasticity of the alloy is 113.8 GPa, Poisson's ratio is 0.342 and the density is 4430 kg/m^3. Damping of the system is modeled as structural damping with a damping coefficient of 2%.

The workpiece dynamics is predicted for each of the ten steps for the strategies described in the previous section. The division for the ten steps along the blade is shown in Figure 5.10. The node which is in contact with the tool in the first step, i.e. at the unmachined stage, can be seen in Figure 5.10. The FRFs of this node for the three strategies described are plotted in Figure 5.11 and Figure 5.12. Note that, x is the feed direction and y is along the thickness direction.

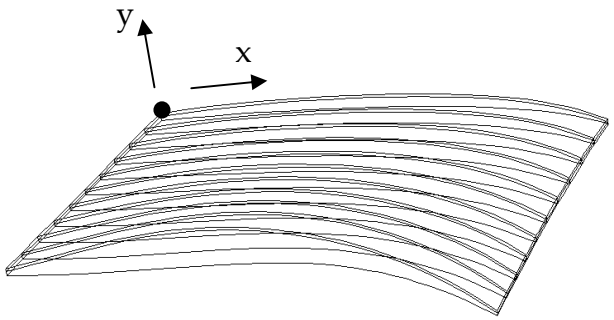

Figure 5.10. The ten steps in finishing of the blade

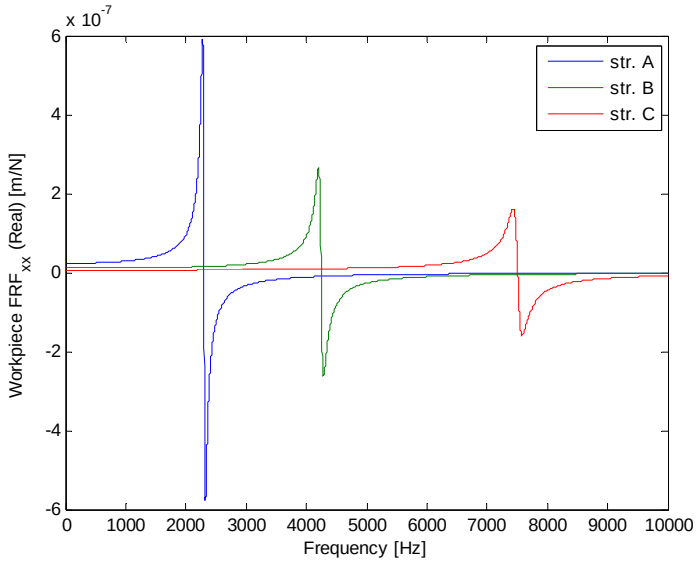

Figure 5.11. Workpiece FRF_{xx} for the first steps in three strategies

Among the three strategies compared, the length of the blade outside hub is the highest in strategy A and it is the lowest in strategy C. The magnitude of the FRF, in x direction, decreases as the length of the blade outside the hub decreases. The value of the first natural frequency is the highest in strategy C.

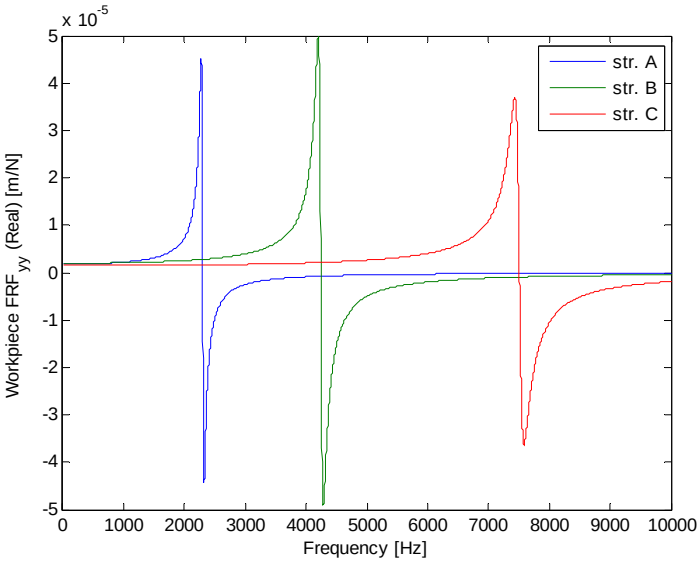

Figure 5.12. Workpiece FRF_{yy} for the first steps in three strategies

The magnitudes of the FRFs in y direction are quite similar for the three strategies, while the frequencies are shifted. These FRFs are used in machining stability to determine the stability limits. The experimentally obtained tool point FRFs, in x and y directions, used in the analysis are shown in Figure 5.13 and Figure 5.14.

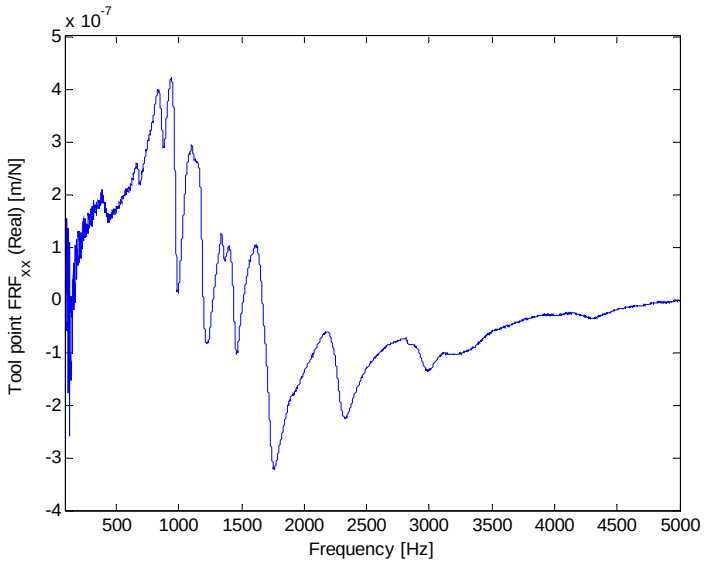

Figure 5.13. Tool point FRF_{xx}

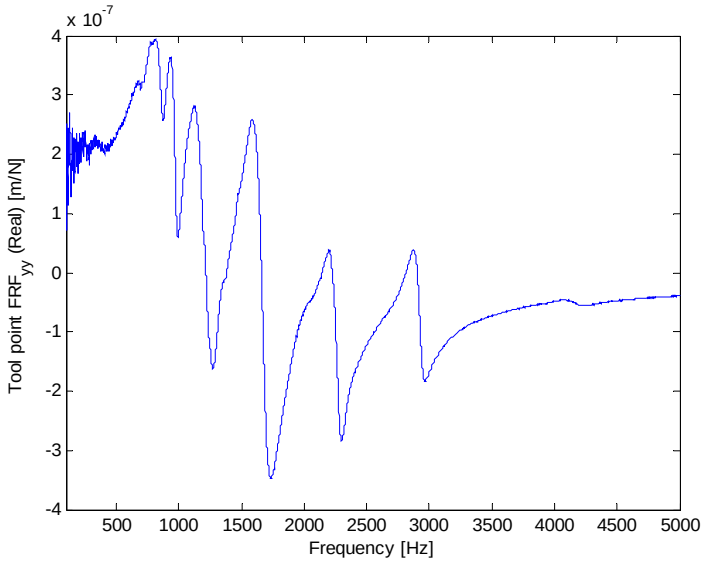

Figure 5.14. Tool point FRF_{yy}

The stability diagrams for the first step for the three strategies are plotted in Figure 5.15. As the machining process goes on in a step, the stability lobes will be shifted. Hence, it is practical to select the limiting depth of cut in these plots as the stable axial depth of cut used in the analysis.

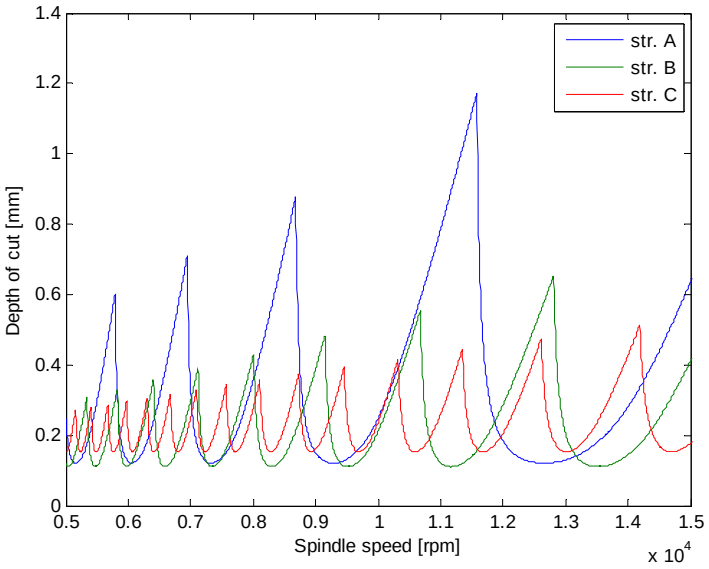

Figure 5.15. Stability lobe diagrams for the first steps in three strategies

Table 5.1 presents the absolute stability limits for axial depths of cut in the ten steps of machining for the production strategies.

Table 5.1. Stability limits, in mm, for the steps in strategies A, B and C

Step	1	2	3	4	5	6	7	8	9	10
A	0.12	0.19	0.35	0.81	2.35	7.23	10.07	9.96	9.95	9.95
B	0.11	0.21	0.70	6.55	9.96	7.23	10.07	9.96	9.95	9.95
C	0.15	0.53	10.28	2.58	10.07	9.95	10.07	9.96	9.95	9.95

The stability limits listed in Table 5.1 show that as the number of steps in the roughing cut increases, more stable cutting occurs.

The average dimensions of the steps on the blade in axial and feed directions, shown in Figure 5.16, are given in Table 5.2.

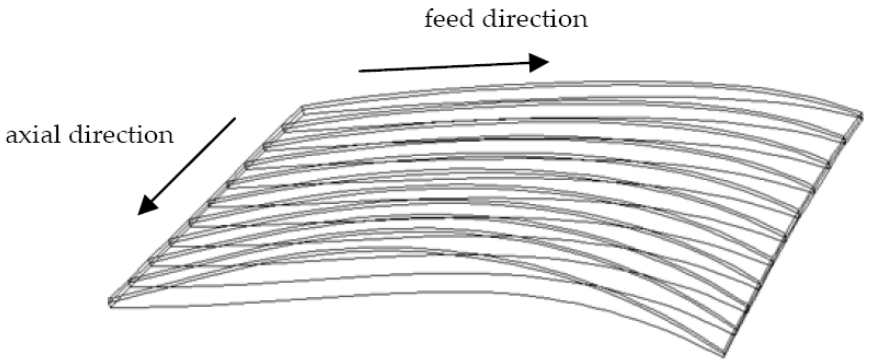

Figure 5.16. Axial and feed directions on the blade

Table 5.2. The lengths of the steps in axial and feed directions

Steps	1	2	3	4	5	6	7	8	9	10
$L_{ax,i}$	5.25	5.20	5.20	5.20	5.20	5.20	5.20	5.20	5.20	5.16
$L_{f,i}$	88.06	86.32	84.97	83.97	83.34	83.12	83.28	83.78	84.56	85.51

The number of passes required to remove the ith step, nop_i, can be calculated by rounding up the ratio of the length of the step in axial direction of the tool ($L_{ax,i}$) to the limiting axial depth of cut in the same step ($a_{\lim,i}$).

$$nop_i = roundup\left(\frac{L_{ax,i}}{a_{\lim,i}}\right) \tag{5.1}$$

The numbers of passes for the steps in each strategy are given in Table 5.3.

Table 5.3. Number of passes in the steps in strategies A, B and C

Step	1	2	3	4	5	6	7	8	9	10
A	44	28	15	7	3	1	1	1	1	1
B	48	25	8	1	1	1	1	1	1	1
C	35	10	1	3	1	1	1	1	1	1

The number of flutes on the tool is four. Spindle speed is taken as 10000 rpm. Feed rate is 0.12 mm/flute. The feed rate in mm/s can be calculated as in equation.

$$V_f = \frac{N \cdot f \cdot n}{60} = \frac{4 \cdot 0.12 \cdot 10000}{60} = 80\ mm/s \tag{5.2}$$

The machining time for one pass at each step can be calculated by dividing the length in feed direction to the feed rate and is tabulated in Table 5.4.

Table 5.4. Machining time, in seconds, for one pass in the steps

Step	1	2	3	4	5	6	7	8	9	10
Time	1.04	1.08	1.06	1.05	1.04	1.04	1.04	1.05	1.06	1.07

The machining time in each step and the total machining time can be calculated for three strategies. Table 5.5 lists the manufacturing times for the strategies.

Table 5.5. Machining time, in seconds, for strategies A, B and C

Step	1	2	3	4	5	6	7	8	9	10	Total
A	45.8	30.2	15.9	7.4	3.1	1.0	1.0	1.1	1.1	1.1	107.7
B	49.9	27.0	8.5	1.1	1.0	1.0	1.0	1.1	1.1	1.1	92.8
C	36.4	10.8	1.1	3.2	1.0	1.0	1.0	1.1	1.1	1.1	57.8

It can be concluded that, dividing the rough cut into two steps decrease the finishing time 14%, and dividing into three steps results in 46% decrease in machining time.

5.3 Effect of the Thickness Removed in Finishing Cut to Productivity

In this section, finishing of the same blade is modeled with the only exception that the thickness removed is 0.25 mm. Strategies labeled as D, E and F, corresponding to the strategies A, B and C in the previous analysis, respectively, will be compared for productivity.

Stable depth of cuts for strategies D, E and F are presented in Table 5.6.

Table 5.6. Stability limits, in mm, for the steps in strategies D, E and F

Step	1	2	3	4	5	6	7	8	9	10
D	0.11	0.17	0.32	0.76	2.22	6.55	13.69	13.43	13.42	13.42
E	0.09	0.16	0.55	5.12	13.43	6.55	13.69	13.43	13.42	13.42
F	0.10	0.32	14.72	2.15	13.73	13.43	13.69	13.43	13.42	13.42

The number of passes required for finishing the steps in strategies D, E and F are given in Table 5.7.

Table 5.7. Number of passes in the steps in strategies D, E and F

Step	1	2	3	4	5	6	7	8	9	10
D	48	31	17	7	3	1	1	1	1	1
E	59	33	10	2	1	1	1	1	1	1
F	53	17	1	3	1	1	1	1	1	1

The machining time calculated for strategies D, E and F are listed in Table 5.8

Table 5.8. Machining time, in seconds, for strategies D, E and F

Step	1	2	3	4	5	6	7	8	9	10	Total
D	49.9	33.5	18.0	7.4	3.1	1.0	1.0	1.1	1.1	1.1	117.2
E	61.4	35.6	10.6	2.1	1.0	1.0	1.0	1.1	1.1	1.1	116.0
F	55.1	18.4	1.1	3.2	1.0	1.0	1.0	1.1	1.1	1.1	84.1

For 0.25 mm thickness removal in the finishing cut, machining times for the strategy with single roughing and the strategy with two steps in roughing are very close. However, for three steps in rough cut, there is 28% decrease in machining time, which shows that the strategy F is the most productive strategy of the strategies considered.

Comparing the results for productivity over the six strategies considered the number of steps in the rough cut improves the productivity. However, the rate of improvement depends on the change in the part dynamics. Stability analysis for different production strategies may reveal more productive cutting.

CHAPTER 6

SUMMARY AND CONCLUSION

In this thesis, the effect of the part dynamics to the machining stability is studied. It is shown both analytically and experimentally that, the stability of a machining process may depend on the workpiece dynamics. The change in part dynamics is predicted by a structural modification method. The effect of material removal to part dynamics is considered.

6.1 Theoretical Background

The change in part dynamics, considering material removal is predicted using a structural modification method. For known dynamics of the original system and the modifying structure, the dynamics of the modified structure is determined. More specifically; using the FRF of the original system and the mass and stiffness matrices of the modifying structure, the FRF of the modified structure is calculated. Matrix inversion is performed in the method. The order of the matrix inverted is equal to the order of the modifying structure, which is generally much smaller than the order of the original structure. This makes the method practical to determine the dynamics of the modified structure, from that of the original structure.

The dynamics of the machined workpiece is obtained by modal analysis on a finite element program. Material removed during machining is considered as modification to the machined workpiece and the dynamics of the unmachined workpiece is predicted. Material removal can be divided into a number of volumes to model the stages of machining. The part dynamics at each stage is predicted by the structural modification method.

Structural modification is applied with additional degrees of freedom. The nodes that belong to the material removal can be divided into two groups: nodes coinciding with those of the original system and the additional nodes. The method applied is practical as the degrees of freedom related with the additional nodes are taken into account.

The method is implemented in Matlab, with two functions. Rearrangement of the elements is required in the method. One of the Matlab function makes this rearrangement. The second function calculates the FRFs of the modified structure.

The material removed during machining is taken as the modifying structure in the modification procedure. The mass and stiffness matrices of the elements representing material removed are required. To make the method more practical, two solid finite elements are modeled. Using these two solid elements, material remoedl can be modeled in three dimensional spaces. For known material properties and geometry, mass and stiffness matrices of the modifying structure are obtained.

6.2 Procedure of Predicting Part Dynamics Considering Material Removal

At the beginning of the procedure, the unmachined geometry is divided into volumes representing material removals and the volume of the machined workpiece. All volumes are modeled using the finite element analysis program Ansys. The modeled volumes are meshed in order to obtain the finite elements on the volumes. The data about these elements are transferred to Matlab in order to be used in the structural modification process. The transferred data include the element numbers on each volume, the node numbers on each element and the coordinates of each node.

The machined geometry is the original structure in the modification procedure. Modal analysis on the machined geometry is performed in Ansys and using the result of this analysis, the FRFs of the structure at different stages of machining operation, as well as the FRF of the original structure are calculated in Matlab. Using the transferred data about the elements, the mass and stiffness matrices of the elements representing the material removed are calculated. These matrices belong to the modifying structure in this procedure. The FRFs of the workpiece, at each stage can be calculated by the modification procedure.

The method implemented is applied to predict the dynamics of different workpiece geometries. The results of the predictions show that the described procedure is accurate to predict the part dynamics at machining stages even for complex geometries like blades.

6.3 Effect of Workpiece Dynamics to Machining Stability

Machining stability analysis is performed on two different workpiece geometries. The first workpiece is a cantilever plate and the second is a blade. For both geometries, different cutting strategies are compared for productivity.

The material of the plate is aluminum. It is modeled as fixed from one its surfaces. Damping of the plate is modeled with proportional structural damping. The machining of the plate is modeled by dividing the material removed into parts in three orthogonal directions. The order of the material removal is determined by the strategy performed. Two different material removal processes are performed: layer removal and step removal. In layer removal, layers of the plate are machined one by one. In step removal, the plate is machined for all layers in one step.

The thickness of the unmachined plate is 9.5 mm and it is decreased to 3 with three layers. The machining stages in three layers are named as roughing, semi-finishing and finishing. Three different layer thickness variations are modeled. In the first thickness variation, the thicknesses are set as 3, 2 and 1.5 mm. In the second and third variation; in order to see the effect of the thicknesses in semi-finishing and finishing stages, to productivity, these thicknesses are decreased and the thickness in roughing is increased.

Three thickness variations are modeled both for layer and step removals, hence a total of six strategies are obtained. For all strategies, part dynamics

at each stage is predicted by the method developed. The predicted FRFs are used in machining stability analysis to obtain stability limits.

Machining stability analysis is performed with the software Cutpro which is a machining simulation program. The dynamics of the tool is included in the analysis with experimentally obtained tool point FRFs. For the conditions specified in section 4.2, the stability analysis is performed.

For unmachined workpiece in strategy A, for the first three successive steps in width direction, stability lobe diagrams have a similar limiting value. Shifting is observed for the stability lobes in the three steps, which makes difficult to determine a common stability over the limiting axial depth of cut. For all strategies, the limiting axial depth of cut is taken as the stability limit in the corresponding step.

For the steps at different positions in height direction, in the first layer, the magnitudes of the FRFs decrease near to the fixed end. This condition results in higher stability limits for the steps near to the fixed end.

Part dynamics at the first step of each layer are also compared and it is observed that the magnitudes of FRFs are higher for thinner workpiece. Hence, the stability limit decreases for thinner workpiece.

Stability limits are derived and listed for all the steps in six strategies. For a selected spindle speed, machining time for one pass is calculated. The number of passes required at each step is also calculated using the stable axial depth of cut at that step. The machining time for each step is obtained

by multiplying the number of passes at the step with the machining time for one pass. The manufacturing times for six strategies are determined.

Comparing the results of the six strategies, step removal is determined to be much productive than layer removal. In layer removal process; increasing the thickness in roughing and decreasing the thickness in semi-finishing and finishing, the machining time increases. In step removal, for higher thickness of the first layer and lower thicknesses of the second and third layers, machining time is lower.

In the second case study, finishing of a blade is analyzed for different strategies in terms of productivity. The blade is cut on a hub in three machining cycles, roughing, semi-finishing and finishing. In roughing, the slots of the blade are obtained. After semi-finishing and finishing cuts, final geometry of the blade is obtained. The blade is more flexible in semi-finishing and finishing cycles than in roughing cycle. The machining productivity depends on the change in workpiece dynamics in semi-finishing and finishing cuts.

Three production strategies are compared for the productivity in finishing cycle. The thickness removed in finishing is taken as 0.5 mm. The difference between the production strategies is the number of stages in roughing cycle. In the first strategy, roughing is performed in a single step. In the second strategy; after half of surface is roughed, it is semi-finished and finished, and then the rest of the blade is machined similarly. In the third strategy, the roughing is divided into three steps.

The machining of the blade surface is divided into ten steps. The change in part dynamics is predicted by the method developed at the ten steps, for three strategies. Machining stability analysis is performed in Cutpro, for the conditions given in Section 5.2. At each step, the limiting depth of cut is taken as the stability limit, since the part dynamics also change along the feed direction.

The machining time for one pass at each of the ten steps is calculated for a spindle speed. The number of passes necessary to machine the material in a step is calculated by dividing the axial length of the step to the axial stability limit. Summation of the manufacturing times at the ten steps gives the finishing time.

Comparing the finishing time for three strategies; the third strategy, in which the roughing is divided into three stages, is found to be the most productive. The manufacturing time for the third strategy is almost half of the time for the strategy with single roughing.

To analyze the productivity for a different value of the thickness removed in finishing cycle, the same blade is modeled for a finishing thickness of 0.25 mm. Similar procedure is applied for this case and the same three strategies are performed.

The results show that dividing the rough cut in three stages is the most productive strategy. The machining time in the third strategy is 28% less than the first strategy.

6.4 General Conclusion

The analytical procedure developed in this study is practical to predict the workpiece dynamics at different stages of machining. It is shown that the change in the dynamics of the workpiece affects the stability of the machining process. At each stage of the machining cycle; in order to determine the stability limit, the dynamics of the workpiece is required to be known. The predictions for the dynamics of workpiece with different geometries are compared and verified with the results of finite element analyses. The procedure developed is practical to be applied to complex three dimensional geometries. Different production strategies can be compared for productivity using the method developed.

6.5 Suggestions for Future Work

Machining stability analysis is performed in this study using the software Cutpro. The FRFs at each machining stage are saved in different files. These files are opened with Cutpro, to represent the part dynamics in the stability analysis. For each stability analysis performed, corresponding file is selected. If the calculations for stability are performed in Matlab, the time spent during file selection will be eliminated and the method will be much practical to use.

REFERENCES

1. Tobias, S. A., *Machine-Tool Vibration*. Blackie & Son Ltd. **1965**

2. Tlusty, J., *Manufacturing Processes and Equipment*. Prentice Hall. **2000**

3. S. A. Tobias, W. Fishwick, '*Theory of Regenerative Machine Tool Chatter*'. The Engineer, 1958. **205**, p. 199-203.

4. S. A. Tobias, W. Fishwick, '*The Chatter of Lathe Tools Under Orthogonal Cutting Conditions*'. Transactions of the ASME, 1958. **80**, p. 1079-1088.

5. Merritt, H. E., '*Theory of Self-excited Machine-tool Chatter*'. Journal of Engineering for Industry, 1965. **87**, p. 447-454.

6. F. Koenigsberger, J. Tlusty, *Machine Tool Structures*. Vol. 1. Pergamon Press. **1970**

7. I. Minis, R. Yanushevsky, '*A New Theorethical Aproach for the Prediction of Machine Tool Chatter in Milling*'. Journal of Engineering for Industry, 1993. **115**, p. 1-8.

8. I. Minis, R. Yanushevsky, Abel Tembo, R. Hocken, '*Analysis of Linear and Nonlinear Chatter in Milling*'. Annals of the CIRP, 1990. **39**(1), p. 459-462.

9. E. Budak, Y. Altıntaş, '*Analytical Prediction of Chatter Stability in Milling - Part II: Application of the General Formulation to Common Milling Systems*'. Transactions of the ASME, 1998. **120**, p. 31-36.

10. E. Budak, Y. Altıntaş, '*Analytical Prediction of Chatter Stability in Milling - Part I: General Formulation*'. Transactions of the ASME, 1998. **120**, p. 22-30.

11. Y. Altıntaş, E. Budak, '*Analytical Prediction of Stability Lobes in Milling*'. Annals of the CIRP, 1995. **44**(1), p. 357-362.

12. U. Bravo, O. Altuzarra, L.N. López de Lacalle, J.A. Sánchez, F.J. Campa, '*Stability Limits of Milling Considering the Flexibility of the*

Workpiece and the Machine'. International Journal of Machine Tools & Manufacture, 2005. **45**, p. 1669-1680.

13. S. Atlar, E. Budak, H. N. Özgüven, *Modeling Part Dynamics and Chatter Stability in Machining Considering Material Removal*, in *1st International Conference on Process Machine Interactions*. 2008: Hannover. p. 61-72.

14. A. Ertürk, E. Budak, H. N. Özgüven, '*Selection of Design and Operational Parameters in Spindle–holder–tool Assemblies for Maximum Chatter Stability by Using a New Analytical Model'*. International Journal of Machine Tools & Manufacture, 2007. **47**, p. 1401-1409.

15. A. Ertürk, H. N. Özgüven, E. Budak, '*Analytical Modeling of Spindle–tool Dynamics on Machine Tools Using Timoshenko Beam Model and Receptance Coupling for the Prediction of Tool Point FRF'*. International Journal of Machine Tools & Manufacture, 2006. **46**, p. 1901-1912.

16. A. Ertürk, H. N. Özgüven, E. Budak, '*Effect analysis of bearing and interface dynamics on tool point FRF for chatter stability in machine tools by using a new analytical model for spindle–tool assemblies'*. International Journal of Machine Tools & Manufacture, 2007. **47**, p. 23-32.

17. E. Budak, A. Ertürk, H. N. Özgüven, '*A Modeling Approach for Analisys and Improvement of Spindle-holder-tool Assembly dynamics'*. Annals of the CIRP, 2006. **55**(369-372).

18. V. Thevenot, L. Arnaud, G. Dessein, G. Cazenave-Larroche, '*Influence of Material Removal on the Dynamic Behaviour of Thin-walled Structures in Peripheral Milling'*. Machining Science and Technology, 2006. **10**, p. 275-287.

19. V. Thevenot, L. Arnaud, G. Dessein, G. Cazenave-Larroche, '*Integration of Dynamic Behaviour Variations in the Stability Lobes Method: 3D Lobes Construction and Application to Thin-walled Structure Milling'*. The International Journal of Advanced Manufacturing Technology, 2006. **27**, p. 638-644.

20. J.V. Le Lan, A. Marty, J.F. Debongnie, '*Providing Stability Maps for Milling Operations'*. International Journal of Machine Tools & Manufacture, 2006. **47**, p. 1493-1496.

21. I. Mañé, V. Gagnol, B. C. Bouzgarrou, P. Ray, '*Stability-based Spindle Speed Control During Flexible Workpiece High-speed Milling*'. International Journal of Machine Tools & Manufacture, 2007. **48**, p. 184-194.

22. K. Weinert, P. Kersting, T. Surmann, D. Biermann, '*Modeling Regenerative Workpiece Vibrations in Five-axis Milling*'. Production Engineering Research and Development, 2008. **2**(3), p. 255-260.

23. J. He, Z.F. Fu, *Modal Analysis*. Butterworth-Heinemann. **2001**

24. Özgüven, H. N., '*Structural Modifications Using Frequency Response Functions*'. Mechanical Systems and Signal Processing, 1990. **4**(1), p. 53-63.

25. R. D. Cook, D. S. Malkus, M. E. Plesha, R. J. Witt, *Concepts and Applications of Finite Element Analysis*. John Wiley & Sons, Inc. **2001**

26. Macneal, R. H., *Finite Elements: Their Design and Performance*. Marcel Dekker, Inc. **1994**